HyShot-T4Supersonic Combustion Experiments

Report for NAG-1-2113

A.Paull, M.Frost and H.Alesi

The Centre for Hypersonics
Dept. of Mechanical Engineering
The University of Queensland, 4072
Australia

TABLE OF CONTENTS

INTRODUCTION

A series of experiments were initiated to investigate the operation of a two-dimensional, hypersonic, air-breathing engine (scramjet) inclined at angles of attack to the freestream. The experiments were undertaken to obtain data for use in the Hyshot flight test program.

Experiments on the Hyshot scramjet were under taken in the T4 shock tunnel. Experiments were made at a nominal total enthalpy of 3.0MJkg^{-1} using a nozzle that produced flows with a Mach number of approximately 6.5. The conditions produced correspond to flight at Mach 7.6 at an altitude range of 35.7 - 21.4km. A summary of the flow conditions is included as Table 1.

The scramjet was tested at 0, plus 2, plus 4, minus 2 and minus 4 degrees angle of attack. Experiments were also undertaken at 2 and 4 degrees angle of skew.

FLIGHT TEST DESCRIPTION

The Hyshot flight program will perform a flight test of a configuration representing a two-dimensional, supersonic combustion ramjet (scramjet) that has also been tested in the T4 shock tunnel. The aim of the Hyshot program is to obtain a correlation between flight based testing and ground based testing in the T4 shock tunnel.

The scramjet will be accelerated to Mach 8 using a Terrier-Orion sounding rocket. The sounding rocket will reach a maximum altitude of 350km. Before re-entry the sounding rocket and scramjet will be maneuvered into the experimental attitude. Between altitudes of 35km and 23km gaseous hydrogen will be injected into the scramjet and pressure measurements will be recorded. A flight Mach No. of 7.6 with a 3-sigma variation of 0.2 is expected.

MODEL CONFIGURATION

Flight and Experimental Model Relationships

A schematic of the flight model and the experimental model is shown as Figure 1. Flight conditions assume a Mach 7.6 flow. The range of freestream pressures and temperatures (P_∞ and T_∞ respectively) expected during flight are deflected by an 18° wedge and are processed the shock system, depicted in Figure 1, to produce a combustion chamber entry temperature of approximately 1100°K and a combustion chamber entrance pressure which ranges between 22kPa and 32kPa. The combustion chamber entry pressures and temperatures (P_o and T_o) are shown in Figure 1.

Experiments in the T4 shock tunnel used a nozzle with a Mach number of 6.5. To reproduce the combustion chamber entrance conditions expected during flight, a 17° compression wedge was used, see Figure 1. The total enthaply of the flow was the same as in flight.

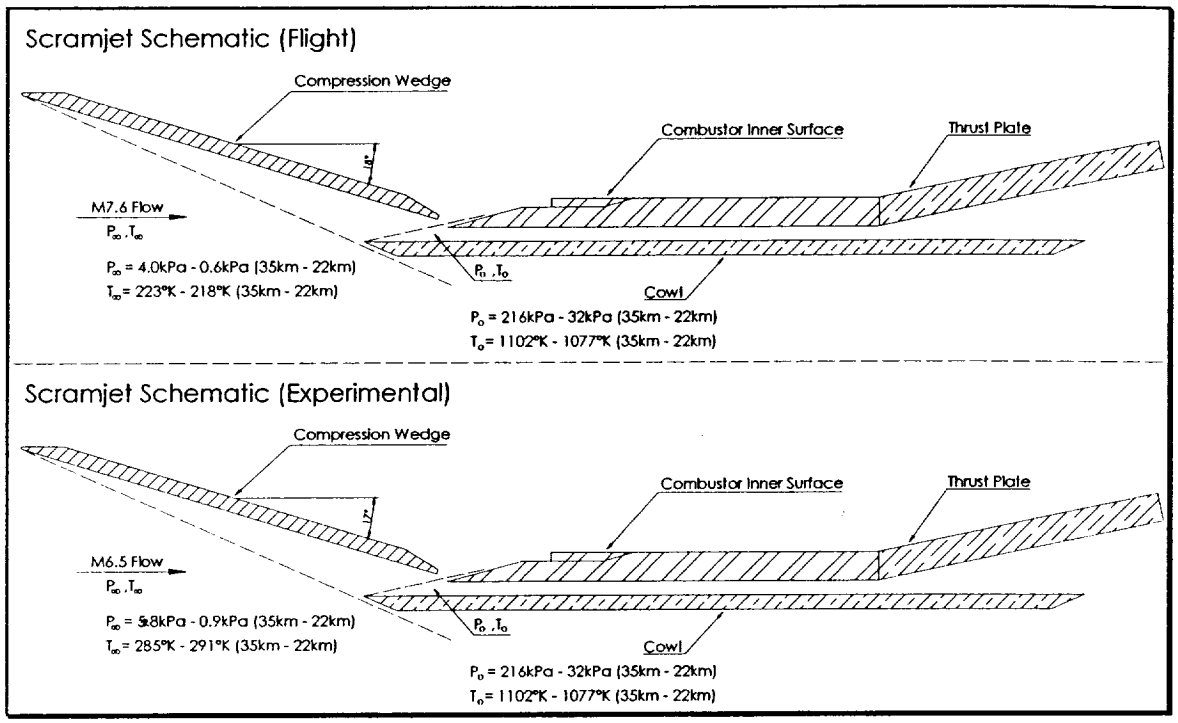

Figure 1 - Hyshot Scramjet Schematic - relationship between the flight model and the experimental model.

General Overview

The engine used in the experiments (Figure 2) features an intake, a combustion chamber and a thrust surface. The intake compresses the freestream using a 17-degree compression wedge. Compressed air from the intake enters the combustion chamber where gaseous hydrogen is injected from porthole injectors located downstream of the combustion chamber entrance. Flow exiting the combustion chamber is expanded over a thrust surface. The experimental model mounted in the test section of the T4 tunnel is shown as Figure 3.

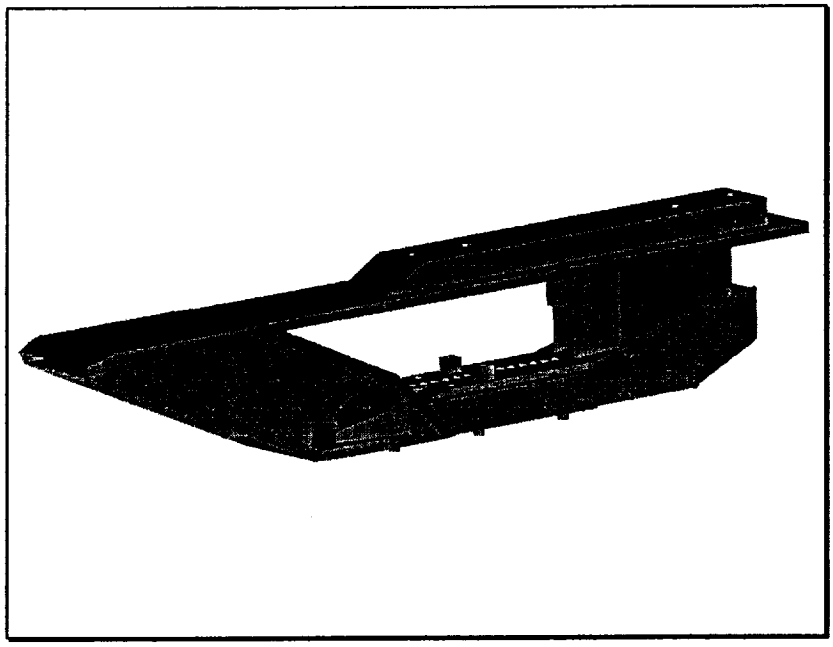

Figure 2 - 3d Model of the Hyshot Scramjet

Intake

The intake is a 17-degree compression wedge, two intake sidewalls and an extension of the intake cowl (Figure 4). The compression wedge is 100mm wide and 305mm long. The leading edge of the compression wedge has been blunted with a 2mm radius. The intake sidewalls are 6mm thick. The leading edges of intake sidewalls have a 20-degree taper perpendicular to the direction of flow and are blunted with a 2mm radius. The intake has been designed so that when operating at between ± 4-degree angle of attack, the flow entering the combustion chamber has uniform temperature, velocity and pressure. This is achieved by allowing shocks generated by the leading edges and the cowl to spill through a gap located between the trailing edge of the compression wedge and the entrance to the combustion chamber. This small gap also bleeds the boundary and entropy layers formed on the compression wedge. Boundary layers formed on the sidewalls are bleed out through cutouts located on the sidewalls. These cutouts have also been designed so that the internal contraction ratio is 1.5. This should allow for self starting of the hyshot experiment. Figure 4, displays a three dimensional representation of the intake assembly.

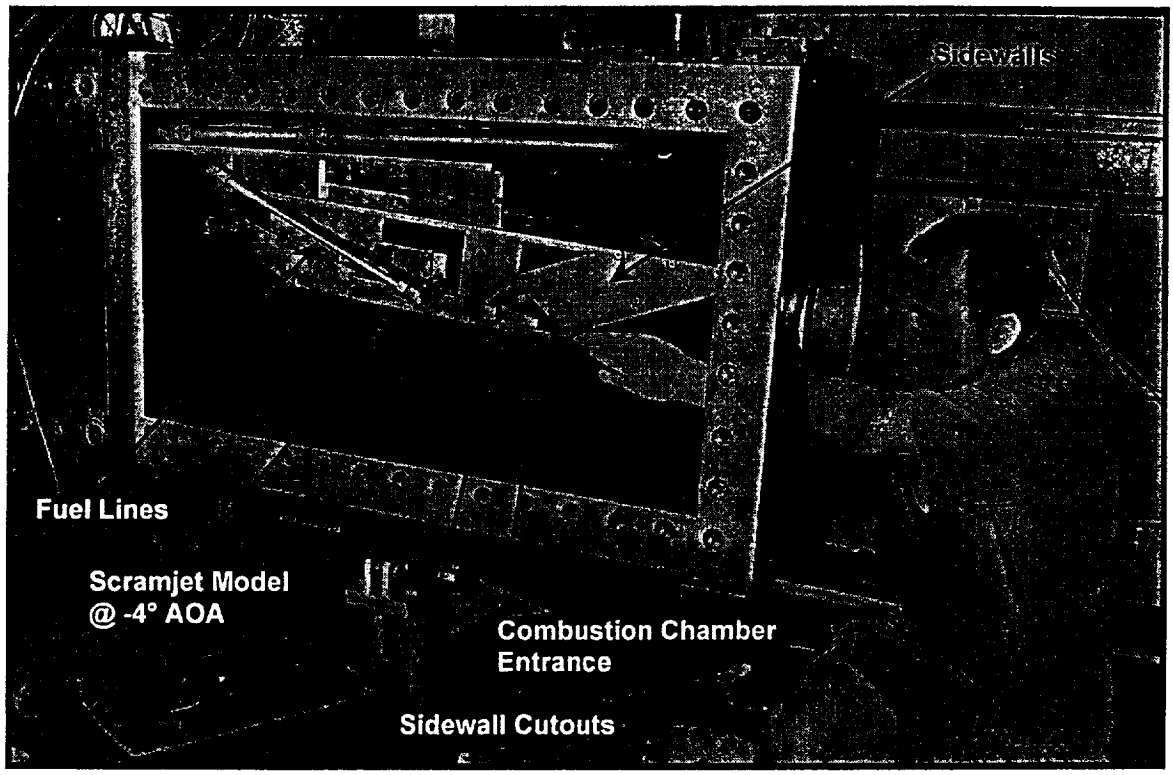

Figure 3 - Hyshot Scramjet Model in T4 Test Section

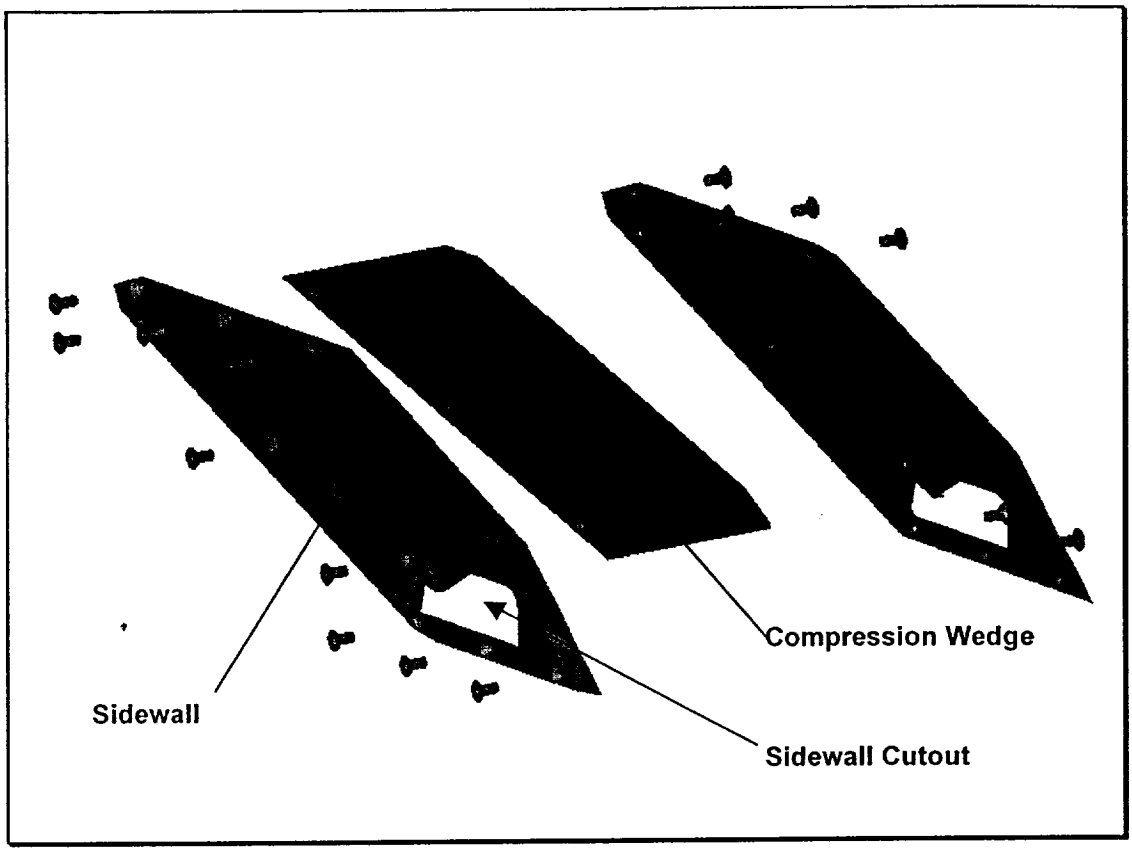

Figure 4 - 3d Model of the Intake Assembly

Combustion Chamber

The combustion chamber is formed from an assembly of the cowl, two sidewalls and an inner surface (Figure 5). The combustion chamber has a constant cross-sectional area and shape throughout its entire length. The chamber is 300mm long, 75mm wide and 9.8mm high. Four 2mm porthole fuel injectors are located 40mm from the leading edge of the inner surface. The injectors inject fuel at 90 degrees to the flow within the combustion chamber. Cavities within the combustor inner surface link the injectors to fuel line connection points. A cutaway of the combustion chamber inner surface (Figure 6) shows the internal fuel cavities and injectors. Pressure transducers are located at 13mm centers along the centerline of the inner surface. The first transducer is located 90mm downstream from the inner surface leading edge. Two additional transducers, located above internal fuel lines, measure the fuel pressure.

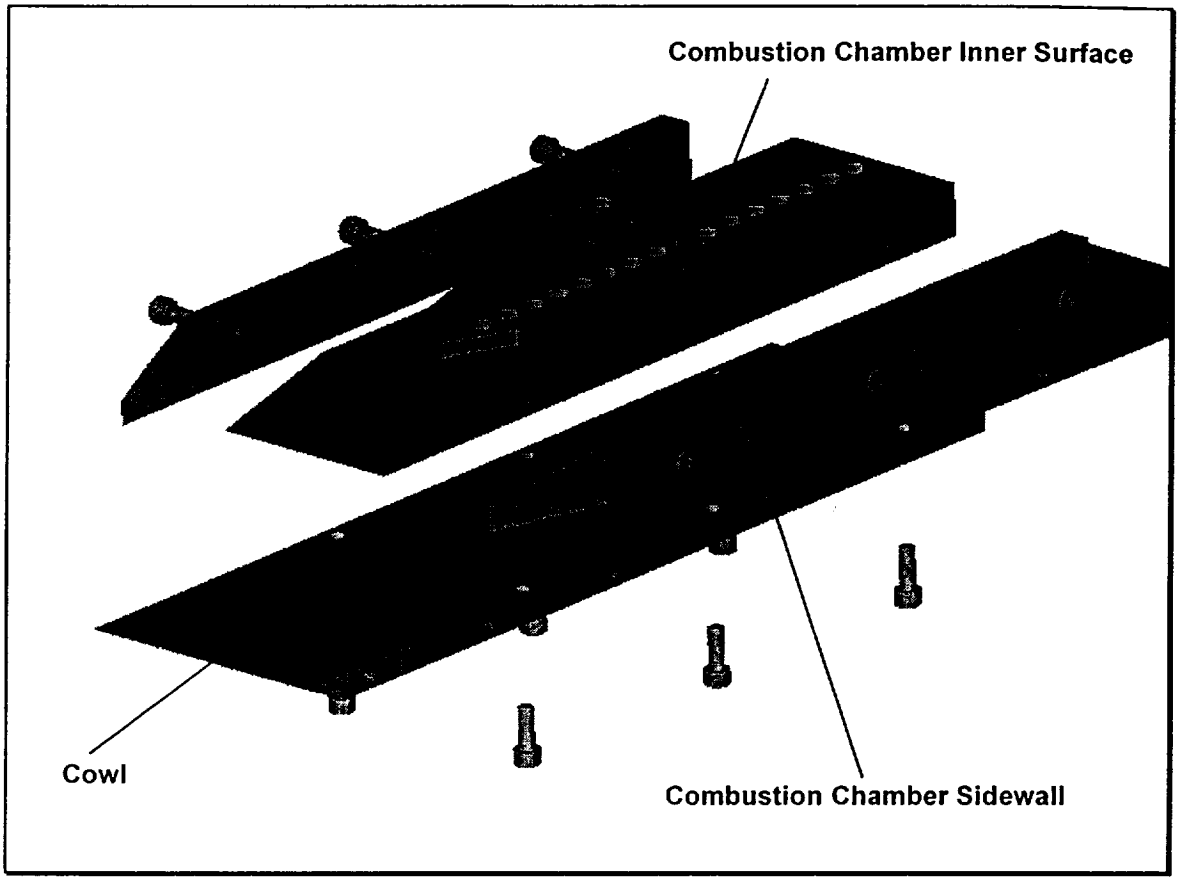

Figure 5 - 3d Model of Combustion Chamber Assembly

Thrust Surface

The thrust surface is formed from a thrust plate inclined at 12 degrees to the combustion chamber inner surface. The thrust plate is 75mm wide and 200mm long. Two side plates connect the thrust plate to the cowl. Pressure transducers are located at 13mm centers along the centerline of the thrust plate. The first transducer is located 11mm from the exit of the combustion chamber. This distance is taken along the length of the thrust surface.

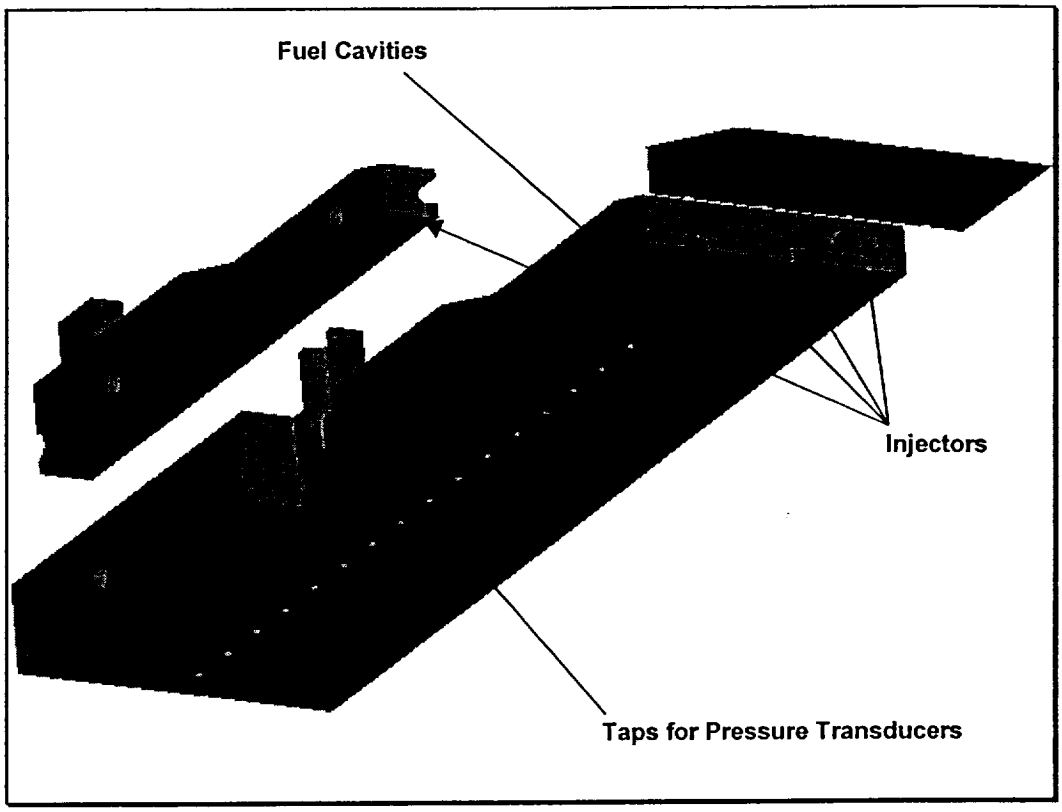

Figure 6 - 3d Cutaway of Combustion Chamber Inner Surface

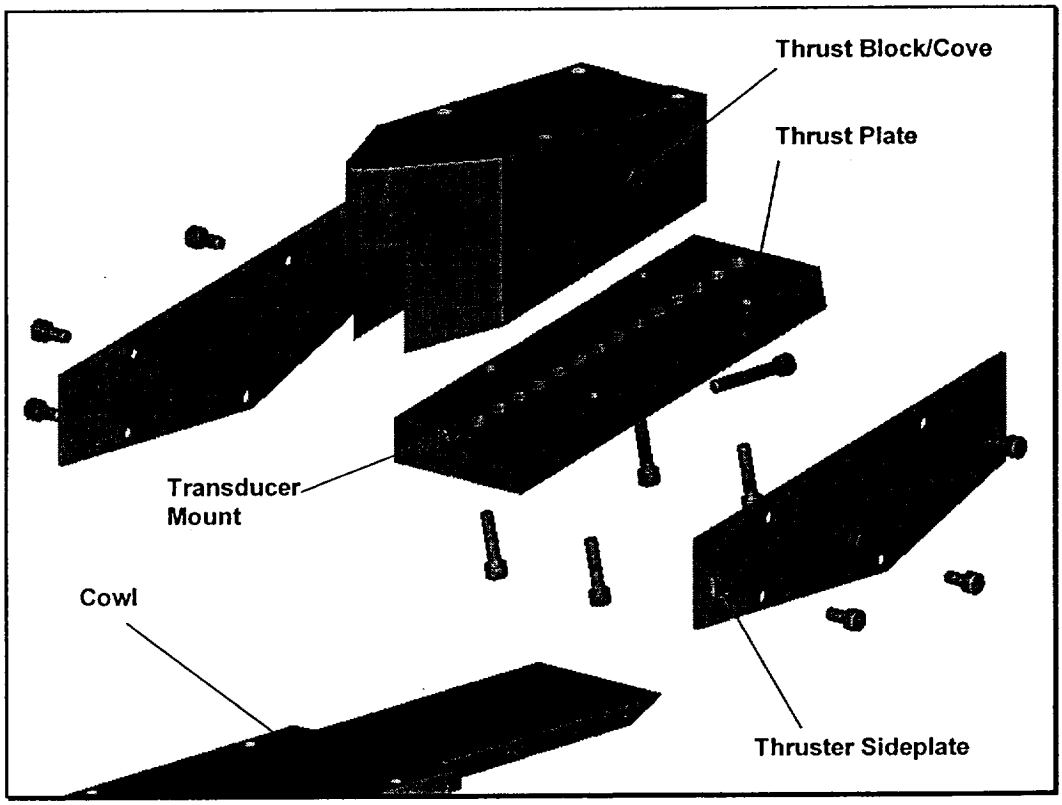

Figure 7 - 3d Thruster Assembly

EXPERIMENTAL MATRIX

Figure 8 is an experimental matrix, which outlines the experiments undertaken. The design condition are defined as 0-degree angle of attack. Angle of attack experiments were undertaken at 2-degrees, 4-degrees, minus 2-degrees and minus 4-degrees. Skew experiments were conducted at 2-degrees and 4-degrees at 0-degree angle of attack. At each angle of attack the equivalence ratio altitude were varied. The typical equivalence range investigated for each angle of attack is shown in Figure 8. The equivalence ranges shown are typical and varied slightly at each altitude tested.

The experimental matrix was repeated for a number of freestream pressures representing altitudes that correspond to expected flight conditions. The compression tube diaphragm thickness was varied to produce the required freestream pressure. A diaphragm thickness of 1mm was used to simulate a nominal altitude of 35km, 2mm for nominal altitude of 28km and 3mm for a nominal altitude of 23km. Experiments were also conducted at design conditions using 4mm diaphragms which corresponded to a nominal altitude of 21km.

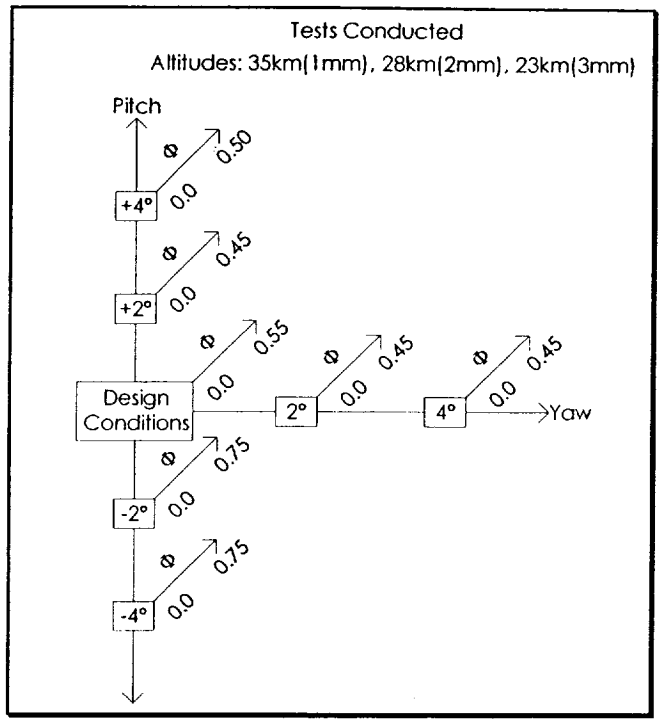

Figure 8 - Experimental Matrix

During the experiments a wedge extension was added to the model to block the small gap between the model base plate and the compression wedge. This extension was added to simulate the symmetry of the flight model. The wedge was removed after observation showed that the wedge did not affect the performance of the scramjet. Also a wedge obstruction was placed between the model base plate and the combustion chamber inner surface to simulate the pressure transducer cover on the flight model. These modifications had no effect in the combustion chamber and thrust surface measurements.

RESULTS

General Overview

The T4 reflected shock tunnel was used for Hyshot scramjet experiments. This facility is located in the Centre for Hypersonics, at the University of Queensland. The T4 facility is a free piston driven shock tunnel. The Hyshot scramjet experiments, reported in this document, used the Mach 6.5 contoured nozzle. Experiments were conducted at a nominal enthalpy of 3.0MJkg^{-1}.

A description of the tests undertaken, including freestream conditions, measured stagnation pressures and shock speeds within the shock tube are included as Table 1 (see appendix A). The freestream conditions, presented in Table 1, have been calculated from the shock speed, stagnation pressure and contour of the nozzle, using the ESTC (McIntosh 1968) and NENZF (Lordi etal 1966) codes.

Pressure measurements were recorded using PCB pressure transducers. Measurements were recorded at a rate of 250kHz on each transducer using a 12bit analog to digital converter. The data was reduced using the UQ program, MONC v4.8.

Fuel Flow Rate

Fuel is supplied to the injectors from the T4 fuel system. The T4 fuel system consists of a Ludwich tube, a fast acting large mass flow rate valve, interconnecting pipe work and associated valving. The Ludwich tube is of sufficient length to supply fuel, at a steady pressure, to the scramjet model for approximately 30 milliseconds. The fast acting fuel valve is located between the Ludwich tube and the injectors.

The fuel system was calibrated by filling the Ludwich tube to a known pressure with gaseous hydrogen. The fast acting fuel valve was then activated and a fuel pressure (FP_m) time history was recorded upstream of the injectors. The pressure within the Ludwich tube after valve activation was also recorded. Assuming the fuel flow is isentropic and adiabatic it can be shown that the mass flow rate of fuel is:

$$\dot{m} = k \times FP_m \times \left(\frac{FP_m}{FP_i} \right)^{0.14}$$

Where FP_i – filling pressure of the Ludwich tube and k is the proportionality constant.

By integrating both sides of the above equation with respect to the time that the valve was opened, and using the change in Ludwich tube pressure to determine the mass of the injected fuel, the proportionality constant, k, can be determined experimentally. The proportionality constant for the Hyshot scramjet experiments was determined to be 1.62×10^8. The error in this measurement was $\pm 3\%$.

Pressure Time History

Figure 9 displays a typical pressure time history for a pressure transducer located in the combustion chamber. The pressure history shown is for transducer number 15, located 272mm downstream from the leading edge of the combustion chamber. This transducer is the second last transducer in the combustion chamber. The chart shows the traces for a fuel off shot (6779) and a fuel on shot (6782). These experiments were conducted at a 0-degree angle of attack and a nominal altitude of 28km. The trace highlights the pressure rise that is associated with combustion.

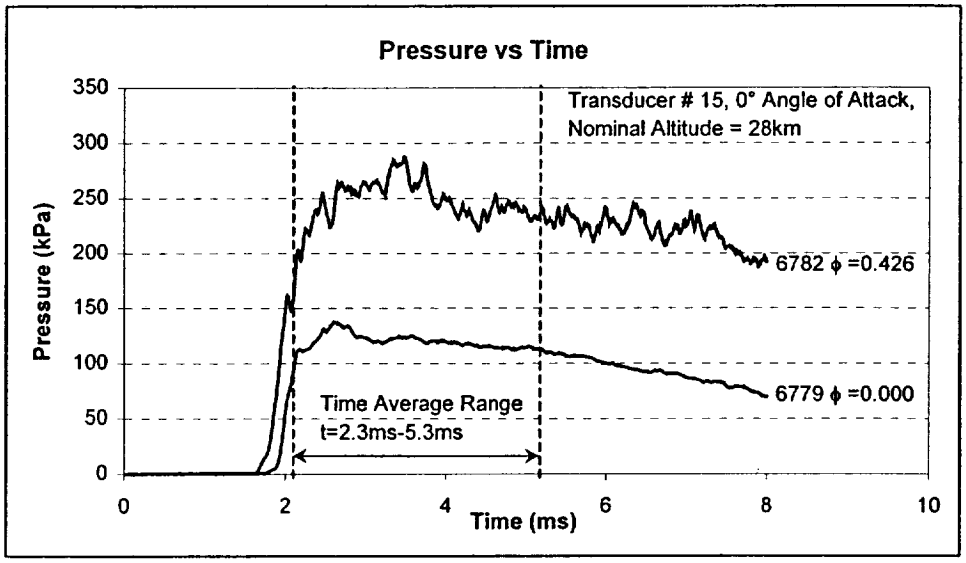

Figure 9 - Typical Pressure Time History

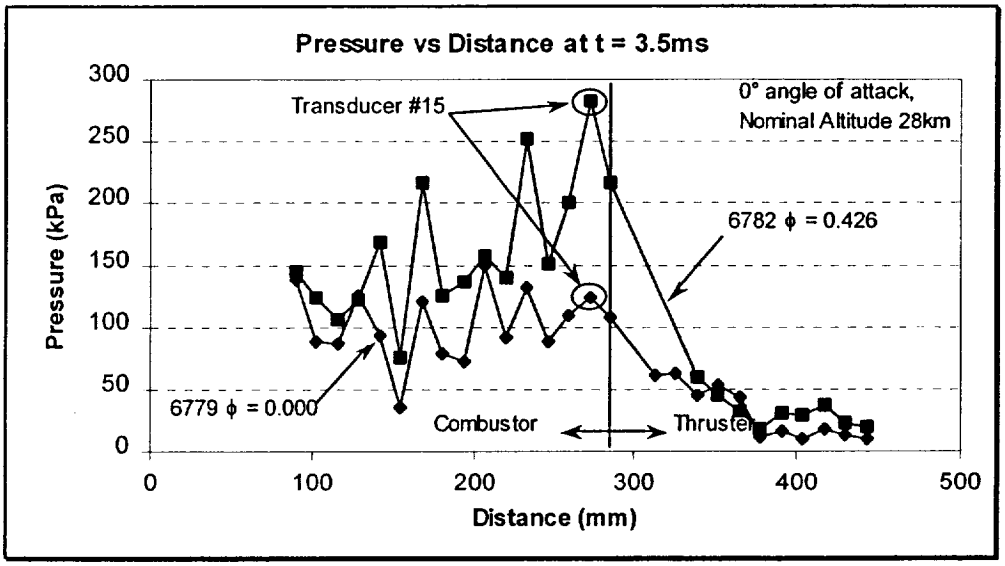

Figure 10 - Pressure vs Distance Plot

Pressure Distance History

0-Degree Angle of Attack

A graph displaying the pressure as a function of distance at t = 3.5ms is shown as Figure 10. Pressure as a function of distance for a fuel off shot (6779) is compared with the pressure as a function of distance for a fuel on shot (6782). These experiments were conducted at a 0-degree angle of attack and a nominal altitude of 28km. Pressure rise due to combustion can be observed, particularly towards the rear of the combustion chamber.

Angle of Attack

A pressure distance history comparison between 4-degree, minus 4-degree and 0-degree angle of attack shots is shown as Figure 11. These shots were conducted at a nominal altitude of 23km with a nominal equivalence ratio of 0.310. At the same nominal equivalence ratio, the 4-degree angle of attack results produced combustion chamber pressures which were greater than the 0-degree angle of attack pressures. Likewise the minus 4-degree angle of attack experiments produced combustion chamber pressures which were lower than the 0-degree angle of attack.

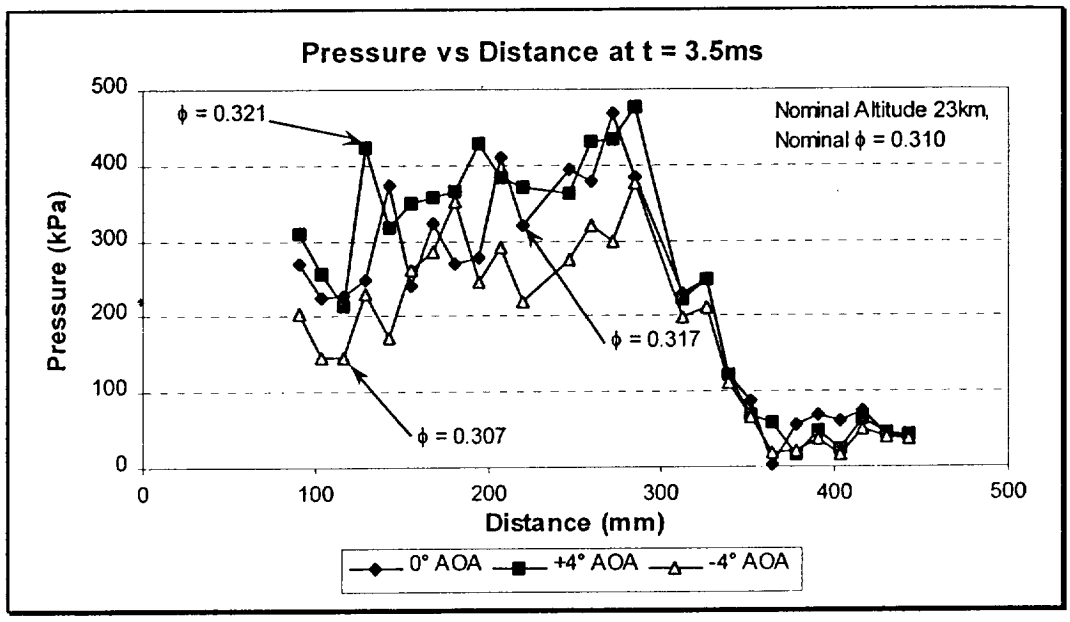

Figure 11 - Pressure vs Distance Angle of Attack Variation

Pressure distance histories for 0-degree, 4-degree and minus 4-degree angles of attack at 35km are shown as Figure 12 - Figure 14. The combustion chamber pressures in these plots have been normalised with the stagnation pressure to eliminate shot to shot variation. The small pressure rise between the fuel off and fuel on experiments at 35km and 0-degree angle of attack indicates that only a small amount of combustion is occurring. Experiments at 4-degree angle of attack and 35 km, Figure 13, displays a much higher pressure rise between the fuel off and the fuel on shots. This trend indicates that combustion is occurring at these conditions. The pressure rise is more noticeable toward the rear of the combustion chamber. The minus 4-degree experiments at 35km showed little pressure rise between the fuel off and fuel on shots indicating that very little, if any, combustion was occurring.

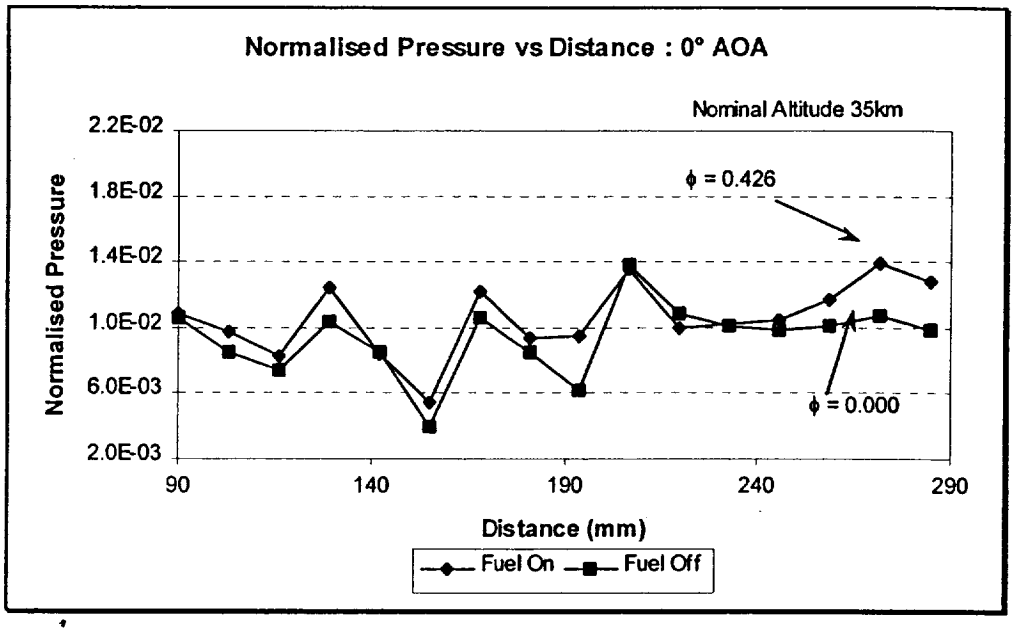

Figure 12 - Normalised Pressure versus Distance for fuel off and fuel on at 0° AOA

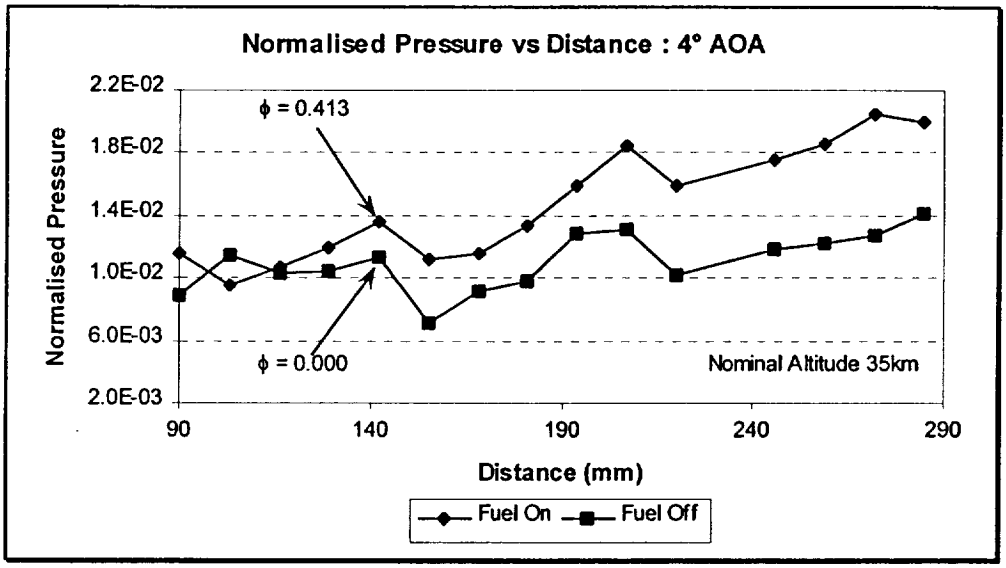

Figure 13 –Normalised Pressure versus Distance for fuel off and fuel on at 4° AOA

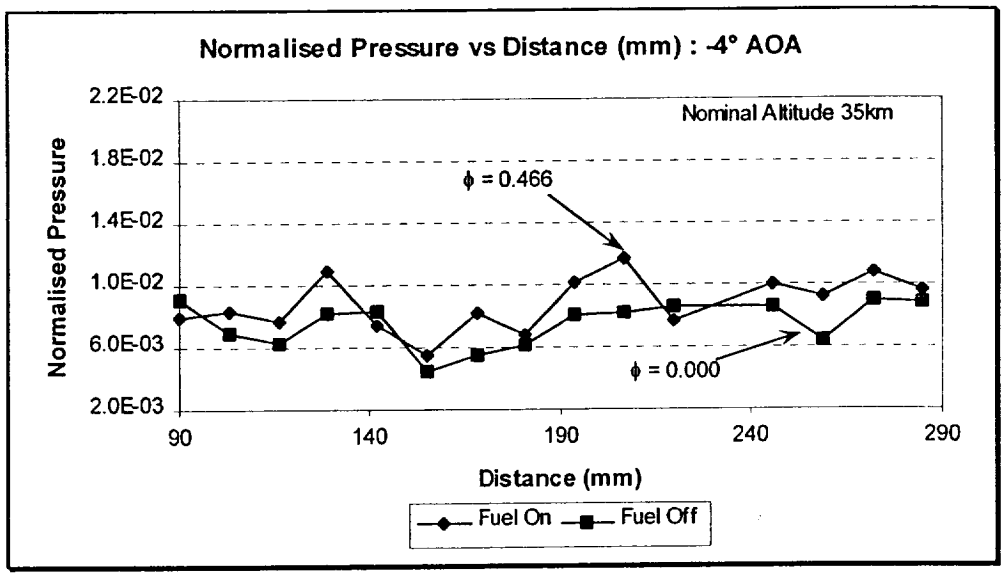

Figure 14 - Normalised Pressure versus Distance for fuel on and fuel off at -4° AOA

4° Angle of Attack and 4° Skew

Analysis of experimental results shows a similarity between 4-degree angle of attack results and 4-degree skew results. Figure 15 displays the relationship between the 4-degree angle of attack pressure distance distribution and the 4-degree skew pressure distance distribution. These experiments were conducted at a nominal altitude of 23km and a nominal equivalence of 0.310.

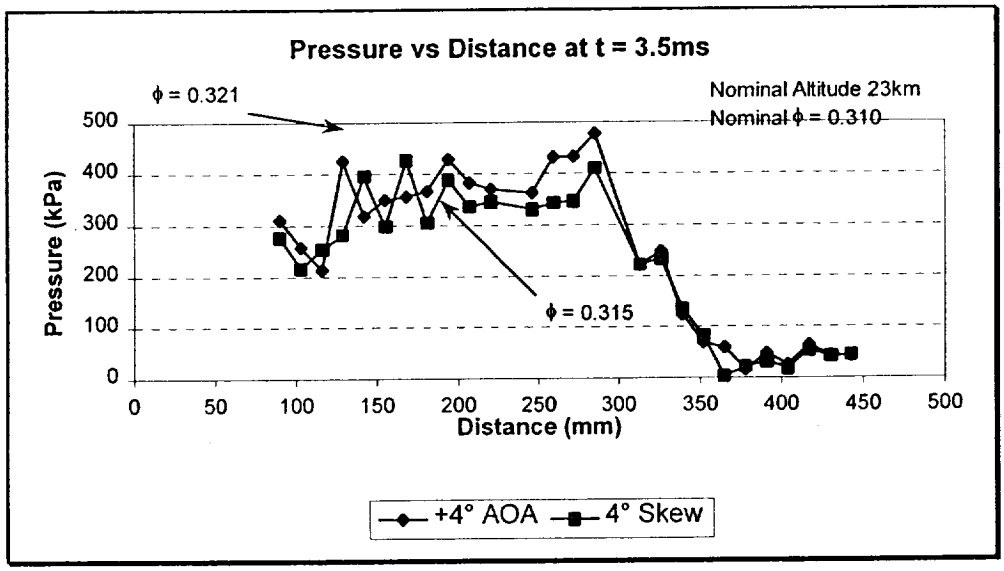

Figure 15 - Pressure vs Distance 4° AOA and 4° Skew

Average Combustion Chamber Pressure

An average combustion chamber pressure has been calculated for all shots. The average pressure is a time average and has been calculated over 3 milliseconds during the test time, see Figure 9. Each pressure transducer in the combustion chamber has been averaged using this method and then an overall average

combustion chamber pressure has been calculated. To eliminate shot to shot variation the overall average has been normalised with respect to the stagnation pressure.

Plots of normalised average combustion chamber pressure versus equivalence are presented as Figure 16 - Figure 18. Each plot displays the normalised average combustion chamber pressure versus equivalence for each altitude tested. These plots show that positive angles of attack have produced greater combustion chamber pressures than those generated at 0-degree angle of attack. Likewise negative angles of attack have produced lower average combustion chamber pressures than those produced at 0-degree angle of attack.

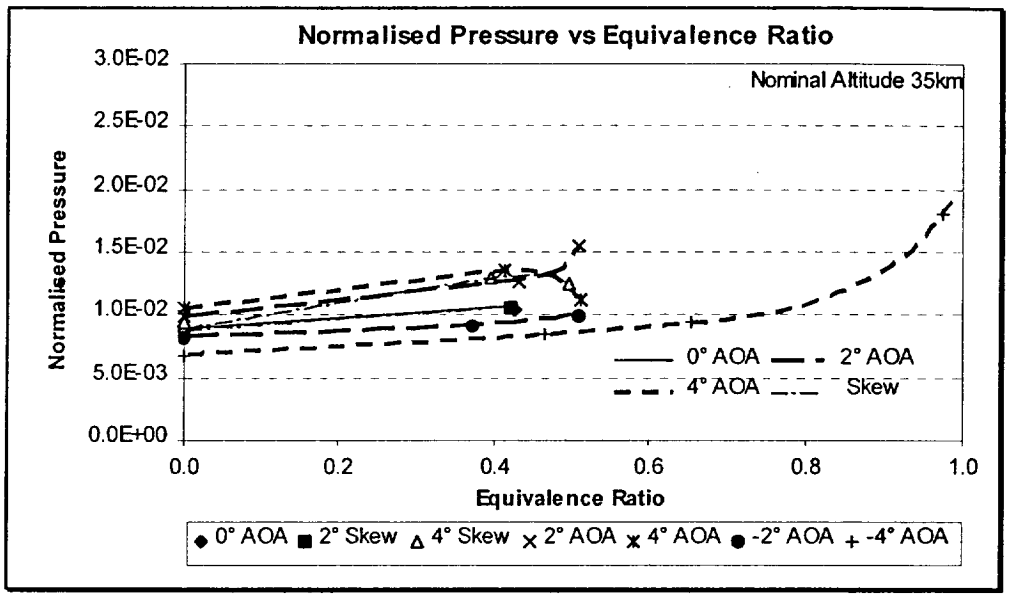

Figure 16 - Normalised Average Combustor Pressure versus Equivalence Ratio at 35km

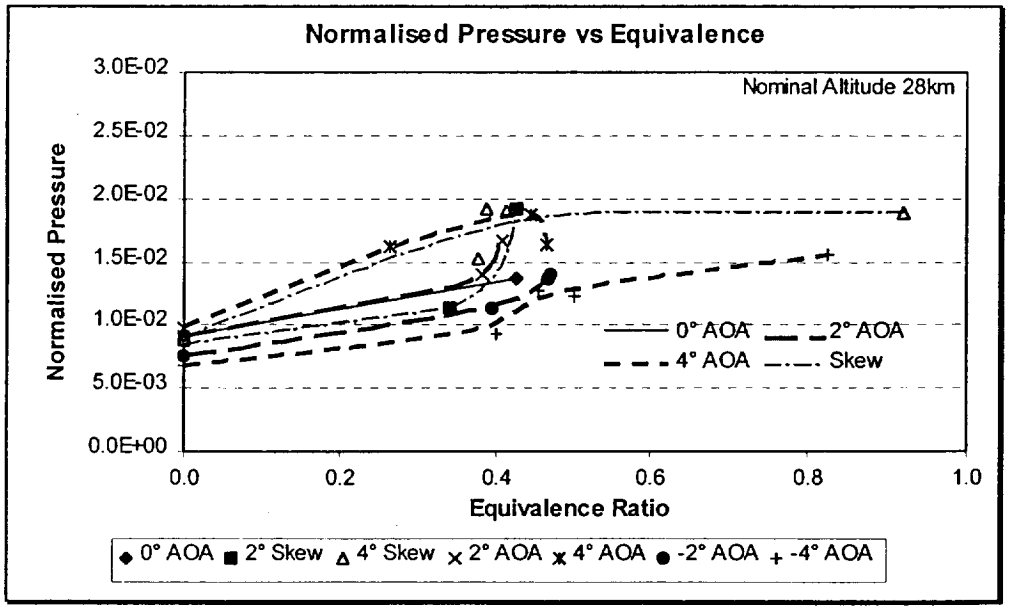

Figure 17 - Normalised Average Combustor Pressure versus Equivalence Ratio at 28km

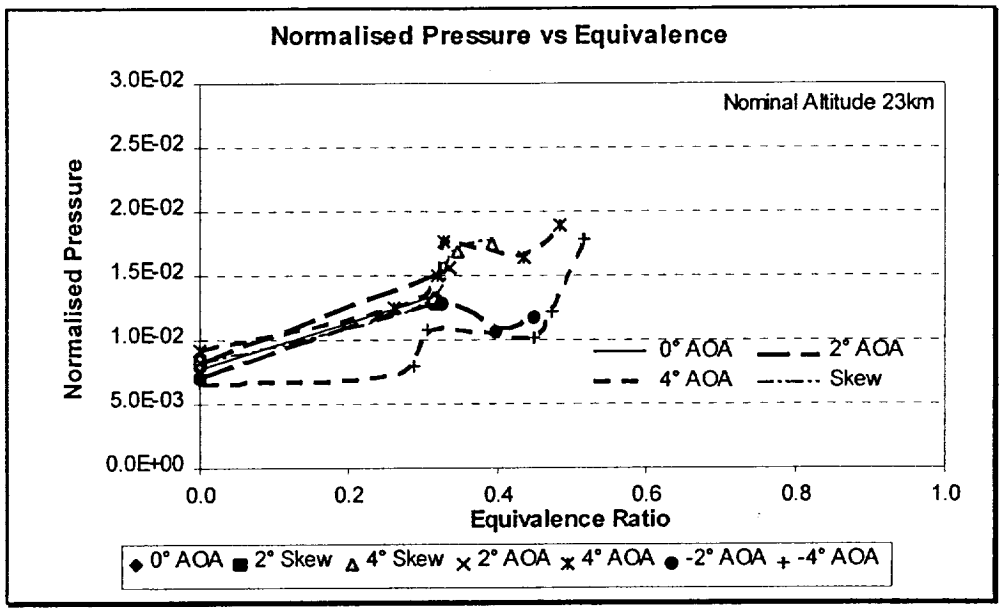

Figure 18 - Normalised Average Combustor Pressure versus Equivalence Ratio at 23km

The average combustion chamber pressure at each angle of attack and angle of skew have been compared to the average combustion chamber pressure at 0-degree angle of attack. These comparisons have been made for fuel off and fuel on shots. Figure 19 - Figure 21 display the average combustion chamber pressure variation from the 0-degree angle of attack average combustion chamber pressures for angles of attack and skew at the altitudes tested. The pressure variation is presented as a percentage of the 0-degree average combustion chamber pressure.

Experiments at positive 2-degree and minus 2-degrees produced average combustion chamber pressures that typically varied by ± 10-20% from the average pressures generated at 0-degree angle of attack. When operating at positive 4-degree and minus 4-degree angle of attack average combustion chamber pressures deviated by ± 15-40% from the average pressures developed at 0-degree angle of attack.

Average combustion chamber pressures formed when operating a 2-degree skew are similar to 0-degree results, except at 28km altitude where the fuel on average combustion chamber pressure was 40% greater than the 0-degree angle of attack average combustion chamber pressure. 4-degree skew average combustion chamber pressures at 23km varied by 10% from the 0-degree average combustion chamber pressures. At an altitude of 28km and with fuel on, the 4-degree average combustor pressures were 40% greater than those produced at 0-degree angle of attack. 4-degree skew average combustion chamber pressures at 35km where 25% greater than the 0-degree angle of attack average combustion chamber pressures.

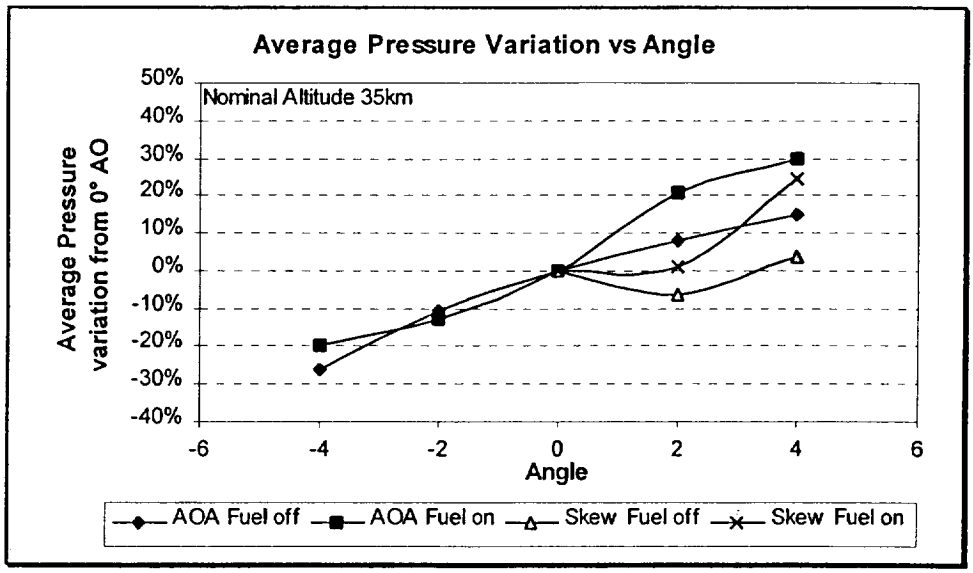

Figure 19 - Average Combustor Pressure Variation at 35km

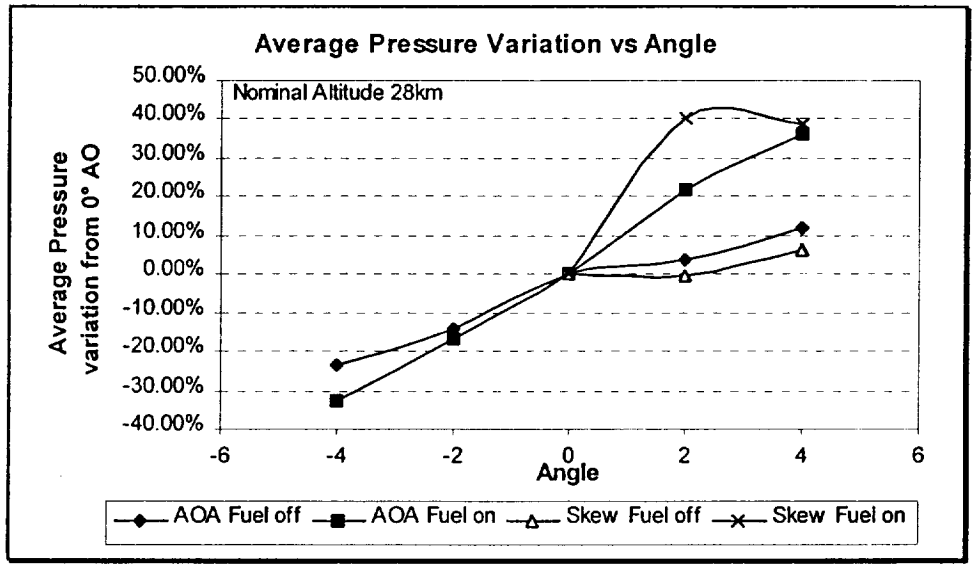

Figure 20 - Average Combustor Pressure Variation at 28km

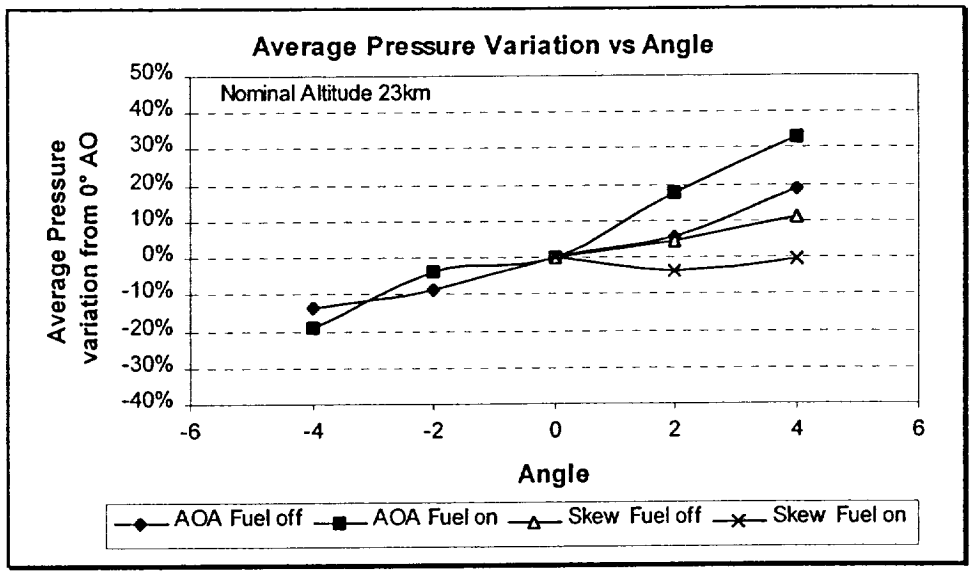

Figure 21 - Average Combustor Pressure Variation at 23km

In general fuel off experiments produced average combustion chamber pressures that varied little from those produced at zero degree angle of attack. The variation was typically 10-15%. The fuel on shots at positive angles of attack produced a greater increase in the average combustion chamber pressure. Negative angles of attack fuel on shots produced combustion chamber pressures that varied only slightly from the average combustion chamber pressures produced during fuel off shots. This trend indicates that positive angles of attack produce combustion chamber conditions that are more favorable for combustion.

Thrust

The thrust produced for each experiment has been calculated by integrating the pressures generated over the thrust surface. To eliminate shot to shot variation the calculated thrusts have been normalised using the stagnation pressure. Figure 22 - Figure 24 displays the normalised thrusts versus the equivalence ratio for each altitude tested.

Skew experiments generally produced the largest thrusts with respect to the 0° angle of attack experiments. Positive angles of attack produced thrusts that were larger than those produced at negative angles of attack. At the 35km and 28km altitudes, positive angles of attack produced thrusts that were larger than those produced at 0-degree angle of attack and the negative angles of attack produced thrusts which were less than those produced at 0-degree angle of attack. At 23km altitude the 0-degree angle of attack produced the largest thrusts. Thrusts produced at all other angles of attack at the 23km altitude varied only slightly.

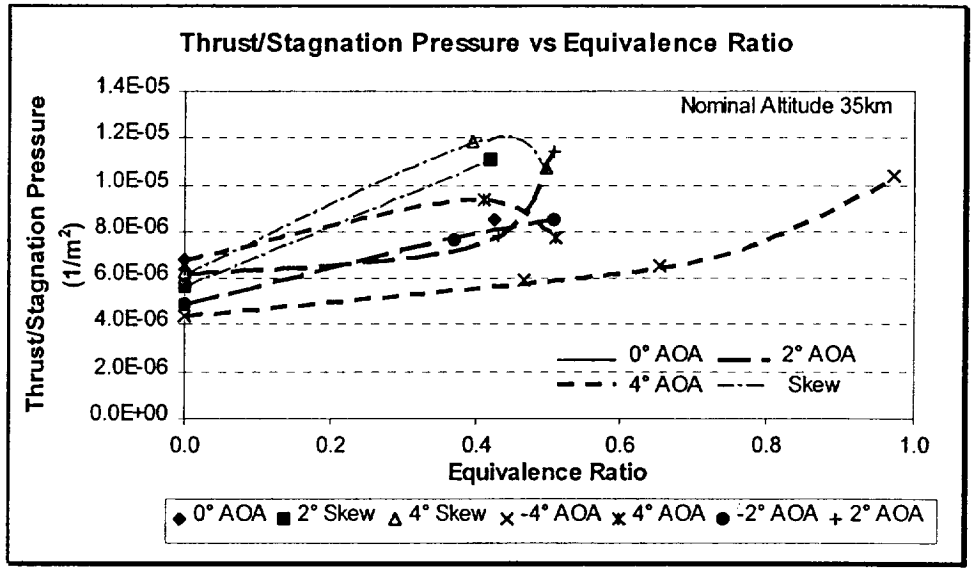

Figure 22 - Thrust/Stagnation Pressure versus Equivalence Ratio at 35km

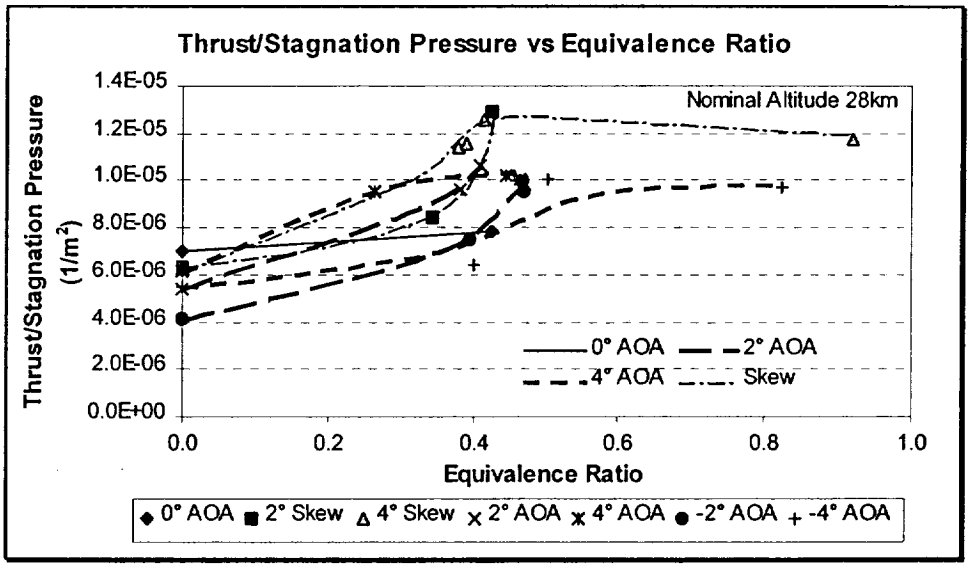

Figure 23 - Thrust/Stagnation Pressure versus Equivalence Ratio at 28km

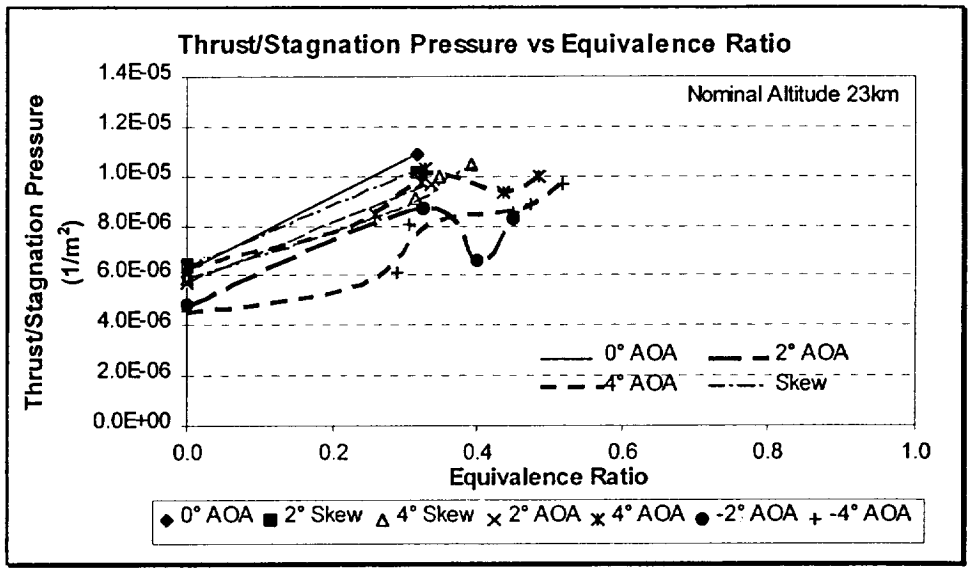

Figure 24 - Thrust/Stagnation Pressure versus Equivalence Ratio at 23km

Boundary Layer Separation

Examining the pressure versus distance time history for all experiments enabled the observation of boundary layer separation. Separation was observed when a pressure disturbance propagated forward through the combustor. This was subsequently associated with a pressure distribution that decreased along the combustor. This decrease in pressure along the combustor has been attributed to subsonic combustion. This trend is shown as Figure 26 – Figure 31. Figure 25 displays the range where boundary layer separation was observed versus altitude. No separation was observed for 4-degree angle of attack, minus 4-degree angle of attack and 4-degree skew experiments.

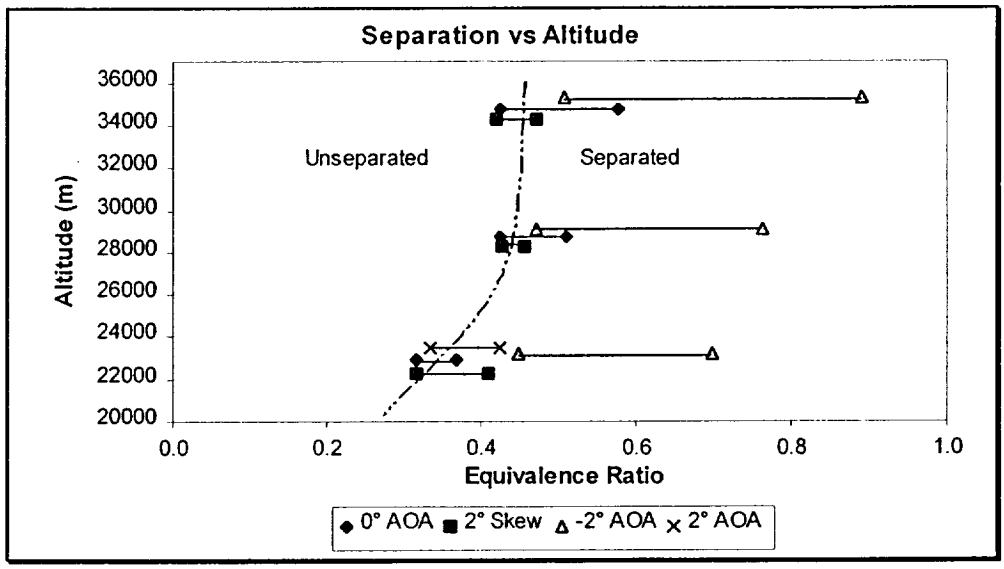

Figure 25 - Separation Equivalence Ratio versus Altitude

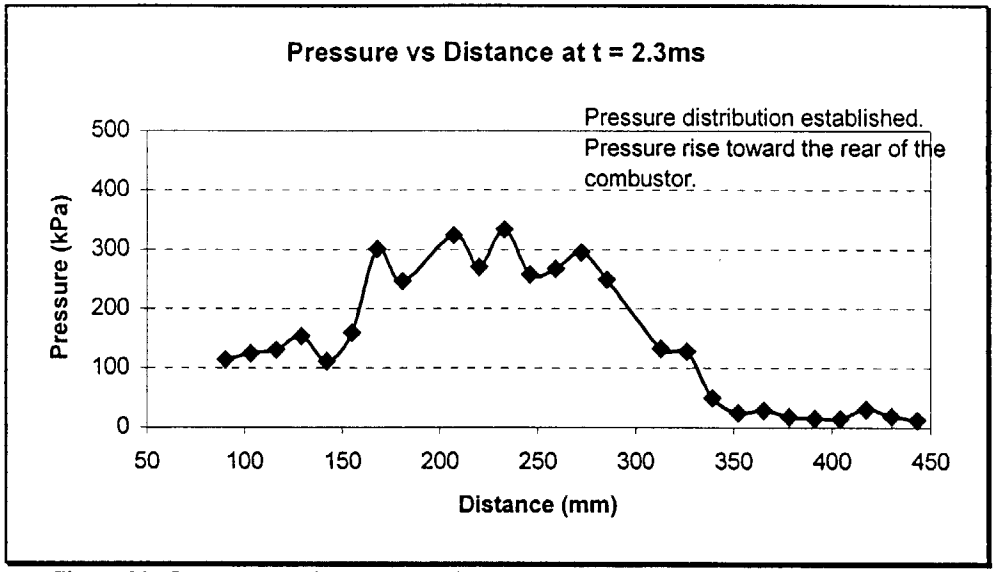

Figure 26 - Pressure vs Distance at t = 2.3ms (Nom. Alt = 28km; AOA = 0°, ϕ = 0.511)

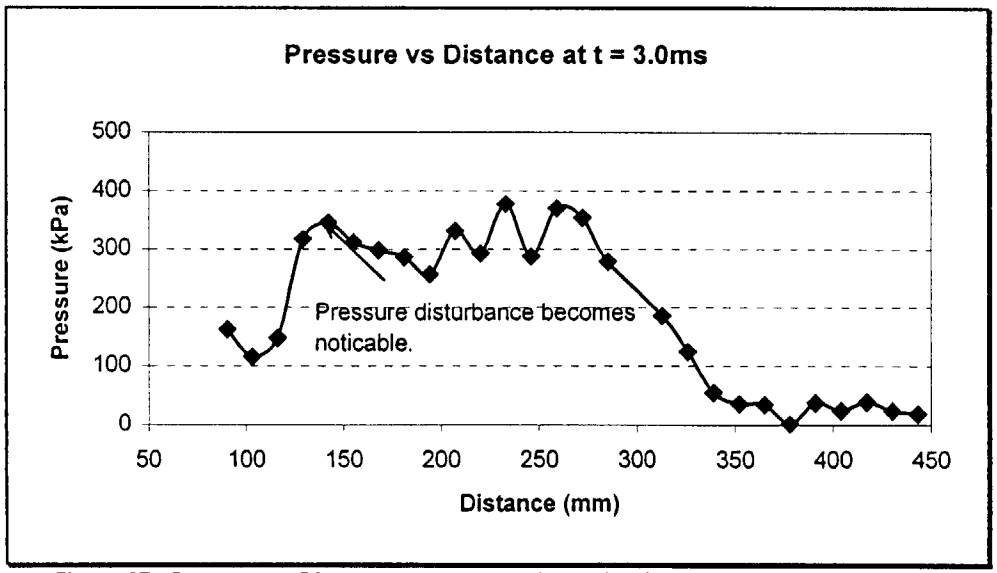

Figure 27 - Pressure vs Distance at t = 3.0ms (Nom. Alt = 28km; AOA = 0°; ϕ = 0.511)

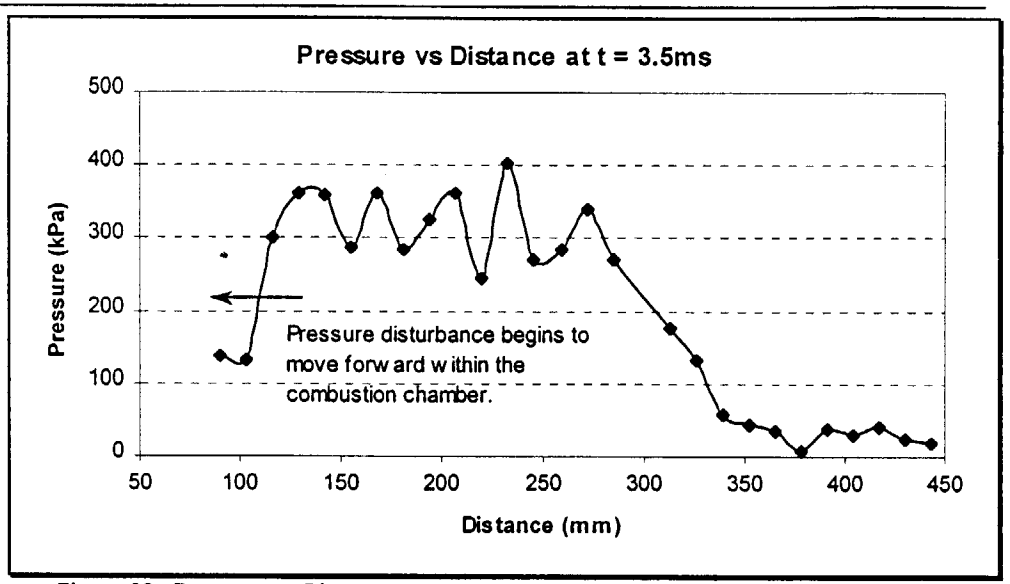

Figure 28 - Pressure vs Distance at t = 3.5ms (Nom. Alt = 28km; AOA = 0°, ϕ = 0.511)

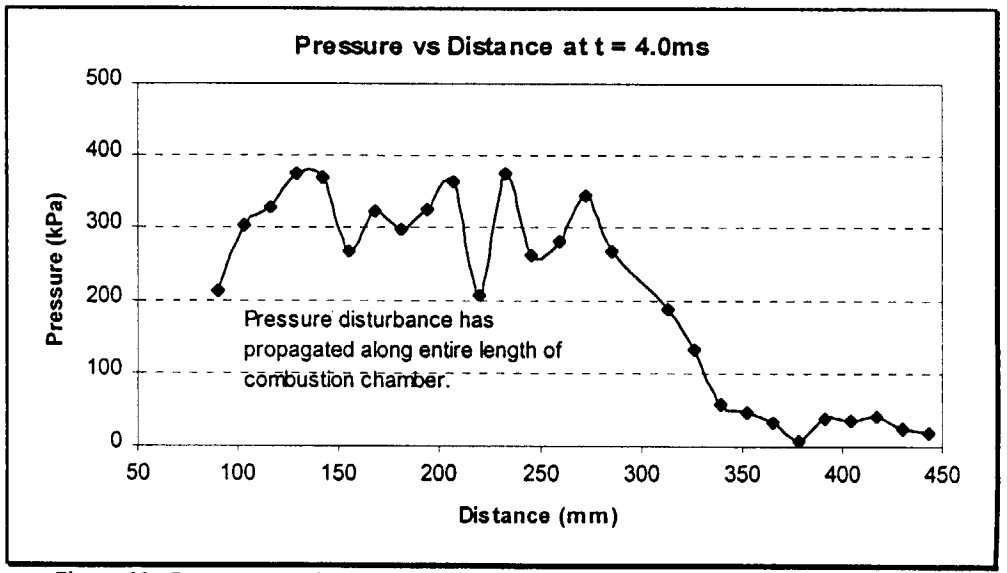

Figure 29 - Pressure vs Distance at t = 4.0ms (Nom. Alt = 28km; AOA = 0°, ϕ = 0.511)

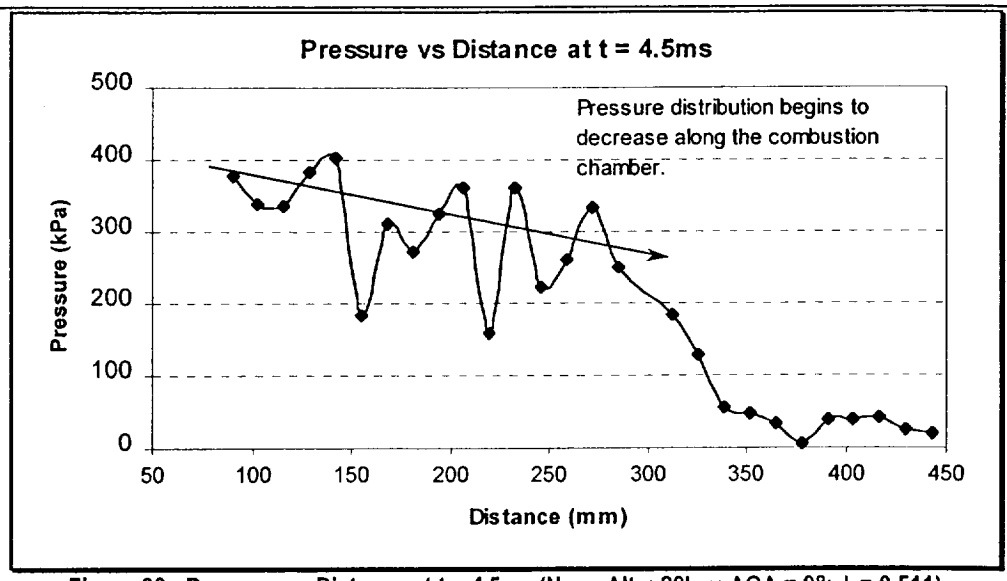

Figure 30 - Pressure vs Distance at t = 4.5ms (Nom. Alt = 28km; AOA = 0°; ϕ = 0.511)

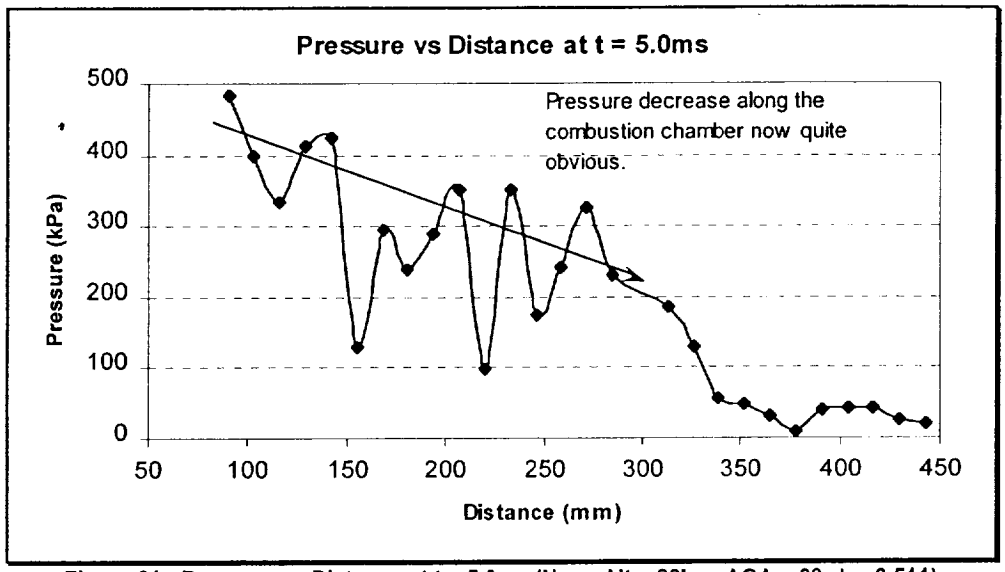

Figure 31 - Pressure vs Distance at t = 5.0ms (Nom. Alt = 28km; AOA = 0°; ϕ = 0.511)

SUMMARY

It is concluded that supersonic combustion was taking place within the combustion chamber. Pressure rises within the combustion chamber were observed during fuel-on shots. Fuel-on shots for low freestream pressures produced combustion towards the rear of the combustion chamber. As the freestream pressure increased, combustion moved forward in the combustion chamber. At high freestream pressures, a pressure rise along the length of the duct indicated combustion was occurring towards the front of the combustion chamber.

Angle of attack tests showed an increase in combustion chamber pressures for positive angle of attacks and a decrease in pressure for negative angles of attack. This result is due to intake shock geometry changes associated with angle of attack operation. 2-degree angle of skew produced combustion chamber pressures which were similar than those produced at 0 degree angle of attack. Thus small changes in skew have a negligible effect on the operation of the scramjet. Positive 4-degree angle of attack experiments produced similar combustion chamber pressures to the 4-degree skew results.

The experimental scramjet operated in a stable manner for equivalences less than 0.4 between altitudes of 35km and 28km. The stability limit decrease to an equivalence of 0.3 at the lower altitude of 23km. No separation was observed when the scramjet operated at 4-degree skew, positive 4-degree and minus 4-degrees angle of attack.

REFERENCES

Lordi, J.A., Mates, R.E., and Moselle, J.R. (1966), **Computer program for the Numerical Solution of Non-equilibrium Expansion of Reacting Gas Mixtures**, *NASA CR-742.*

McIntosh, M.K. (1968), **Computer Program for the Numerical Calculation of Frozen and Equilibrium Conditions in Shock Tunnels**, *Dept of Physics, ANU Report.*

TABLE 1 – RUN SUMMARY

Run Number	Diaphram	Freestream Pressure	Freestream Temperature	Freestream Velocity	Pitot Pressure	Mach Number	Total Entalpy	Angle of Attack	Angle of Slew	Fuel Pressure Fpm	Initial Fuel Pressure Fpi	Shock Tube Fill Pressure	Stagnation Pressure	Shock Speed	Flight Pressure	Flight Temperature	Flight Altitude
Units	mm	kPa	K	ms^{-1}	kPa	-	$MJkg^{-1}$	degree	degree	kPa	kPa	kPa	MPa	kms^{-1}	kPa	K	m
6805	4	6.343	278	2284.0	420.30	6.833	2.888	0	0	1440	1725	320	33.498	1.65	4.471	226	21360
6802	4	6.282	282	2295.2	422.90	6.822	2.920	0	0	1686	2180	320	33.052	1.73	4.413	229	21444
6775	4	6.212	278	2284.0	450.30	6.833	2.890	0	0	1110	1290	300	32.809	1.72	4.379	226	21494
6773	4	6.234	283	2301.0	415.70	6.818	2.930	0	0	2475	3155	300	32.758	1.74	4.372	229	21504
6771	4	5.986	286	2294.5	462.10	6.766	2.920	0	0	0	0	300	29.917	1.74	4.131	229	21869
6772	4	5.813	288	2316.5	454.40	6.803	2.970	0	0	2055	2580	300	30.398	1.76	4.056	232	21987
6845	3	5.791	306	2290.2	303.60	6.531	2.930	4	0	959	1130	200	23.383	1.70	3.778	233	22445
6833	3	5.943	319	2327.7	662.80	6.499	3.030	0	4	1174	1400	200	23.546	1.74	3.757	244	22480
6834	3	5.850	300	2272.7	745.10	6.546	2.884	0	4	1270	1770	200	23.546	1.69	3.753	231	22488
6816	3	5.741	309	2300.3	716.90	6.522	2.957	0	2	1164	1400	200	22.910	1.72	3.658	237	22653
6817	3	5.720	309	2300.3	719.30	6.522	2.957	0	2	1532	1870	200	22.829	1.72	3.645	237	22677
6835	3	5.698	306	2291.8	702.10	6.529	2.935	0	4	1424	1870	200	22.798	1.71	3.636	235	22692
6865	3	5.691	305	2286.5	302.10	6.534	2.921	4	0	1451	1870	200	22.808	1.70	3.627	232	22708
6842	3	5.514	297	2266.3	301.70	6.551	2.867	4	0	1166	1400	200	22.234	1.69	3.623	227	22715
6843	3	5.686	306	2291.8	306.60	6.529	2.933	4	0	1150	1360	200	22.747	1.71	3.617	232	22726
6873	3	5.770	319	2325.6	304.10	6.501	3.024	-2	0	1179	1400	200	22.863	1.75	3.608	245	22742
6796	3	5.568	308	2295.0	210.40	6.527	2.942	0	0	0	0	200	22.261	1.72	3.605	236	22748
6797	3	5.650	308	2297.1	105.20	6.525	2.947	0	0	1889	2335	200	22.575	1.72	3.605	236	22748
6807	3	5.603	302	2278.0	699.30	6.541	2.897	0	0	1162	1400	200	22.514	1.69	3.594	232	22767
6841	3	5.457	297	2265.3	299.70	6.553	2.863	4	0	1166	1400	200	22.031	1.68	3.588	227	22778
6815	3	5.626	310	2302.4	719.10	6.521	2.961	0	2	0	0	200	22.454	1.72	3.583	238	22786
6818	3	5.616	308	2295.0	718.90	6.527	2.942	0	2	1484	1720	200	22.454	1.71	3.581	236	22791
6871	3	5.690	311	2304.0	304.00	6.519	2.966	-2	0	1641	1870	200	22.693	1.72	3.569	239	22812
6872	3	5.617	305	2288.6	305.60	6.532	2.926	-2	0	1399	1770	200	22.502	1.71	3.544	236	22858
6881	3	5.467	305	228.7	308.40	6.532	3.061	2	0	0	0	200	21.900	1.72	3.537	233	22870
6806	3	5.494	298	2268.5	695.10	6.550	2.873	0	0	1322	1635	200	22.150	1.69	3.530	230	22884
6870	3	5.584	309	2299.3	303.40	6.524	2.954	-2	0	0	0	200	22.312	1.72	3.510	238	22919
6801	3	5.468	301	2277.0	279.10	6.543	2.894	0	0	1480	1870	200	21.991	1.70	3.510	232	22920
6799	3	5.465	307	2294.0	279.00	6.528	2.940	0	0	1494	1870	200	21.866	1.72	3.485	236	22966
6850	3	5.583	303	2282.3	276.50	6.538	2.908	-4	0	1015	1130	200	22.422	1.70	3.480	236	22975
6851	3	5.581	303	2281.7	276.00	6.538	2.908	-4	0	1056	1400	200	22.402	1.70	3.479	250	22977
6840	3	5.228	291	2248.2	289.40	6.568	2.819	4	0	0	0	200	21.223	1.68	3.452	223	23028

TABLE1 – RUN SUMMARY

Run Number	Diaphram	Freestream Pressure	Freestream Temperature	Freestream Velocity	Pitot Pressure	Mach Number	Total Entalpy	Angle of Attack	Angle of Slew	Fuel Pressure Fpm	Initial Fuel Pressure Fpi	Shock Tube Fill Pressure	Stagnation Pressure	Shock Speed	Flight Pressure	Flight Temperature	Flight Altitude
Units	mm	kPa	K	ms^{-1}	kPa	-	$MJkg^{-1}$	degree	degree	kPa	kPa	kPa	MPa	kms^{-1}	kPa	K	m
6883	3	5.295	296.45	2262.6	299.30	6.554	2.858	2	0	1428	1770	200	21.380	1.69	3.446	227	23038
6800	3	5.337	295	2258.9	280.80	6.558	2.847	0	0	1780	2100	200	21.572	1.68	3.441	228	23049
6854	3	5.524	309	2296.6	270.70	6.525	2.946	-4	0	1618	1870	200	22.071	1.72	3.420	239	23089
6884	3	5.215	297	2264.2	301.30	6.553	2.862	2	0	1137	1400	200	21.042	1.70	3.393	228	23141
6864	3	5.206	309	2299.8	307.80	6.522	2.955	4	0	1590	1870	200	20.782	1.72	3.390	234	23146
6830	3	5.210	289	2240.7	678.20	6.574	2.801	0	4	0	0	200	21.183	1.67	3.375	224	23174
6831	3	5.118	272	2188.3	662.80	6.618	2.668	0	4	633	1400	200	21.127	1.60	3.364	212	23195
6900	3	5.325	305	2287.6	293.50	6.534	2.923	-2	0	2350	3200	200	21.358	1.72	3.364	250	23196
6852	3	5.357	295	2258.9	271.30	6.558	2.847	-4	0	1489	1770	200	21.654	1.68	3.353	230	23216
6882	3	5.107	288	2236.4	295.60	6.577	2.790	2	0	1631	1870	200	20.777	1.67	3.349	222	23225
6848	3	5.258	290	2243.9	267.80	6.570	2.808	-4	0	0	0	200	21.348	1.67	3.309	227	23302
6832	3	5.016	271	2185.1	675.80	6.620	2.659	0	4	783	1400	200	20.726	1.60	3.300	212	23320
6896	3	5.251	304	2283.9	286.10	6.537	2.913	-4	0	1674	2150	200	21.078	1.72	3.272	236	23375
6853	3	5.692	309	2298.1	275.80	6.524	2.950	-4	0	1343	1870	200	22.728	1.71	2.904	207	24151
6886	2	2.694	329	2354.4	150.50	6.476	3.102	2	0	646	980	90	10.584	1.77	1.853	268	26992
6811	2	2.786	314	2313.1	-	6.511	2.990	0	2	623	940	90	11.075	1.71	1.767	240	27292
6783	2	2.586	310	2301.0	136.40	6.522	2.960	0	0	1032	1240	90	10.326	1.72	1.539	248	28198
6779	2	2.235	298	2332.1	145.80	6.733	3.020	0	0	0	0	90	11.045	1.72	1.524	237	28263
6782	2	2.620	311	2305.8	139.10	6.517	2.979	0	0	701	940	90	10.444	1.70	1.522	249	28273
6866	2	2.676	310	2302.0	144.30	6.520	2.962	4	0	0	0	90	10.659	1.71	1.454	235	28574
6867	2	2.791	323	2338.5	152.00	6.489	3.058	4	0	785	980	90	11.015	1.74	1.439	243	28642
6869	2	2.810	324	2340.1	151.50	6.488	3.063	4	0	428	760	90	11.085	1.74	1.438	244	28646
6829	2	2.582	299	2270.6	334.90	6.548	2.878	0	4	645	760	90	10.403	1.68	1.435	230	28662
6885	2	2.662	317	2320.6	149.70	6.505	3.010	2	0	0	0	90	10.564	1.73	1.433	250	28669
6868	2	2.896	331	2360.1	153.90	6.469	3.118	4	0	770	940	90	11.341	1.76	1.431	249	28681
6827	2	2.622	304	2285.5	344.80	6.534	2.918	0	4	643	940	90	10.511	1.69	1.429	234	28687
6785	2	2.607	306	2291.4	133.60	6.531	2.932	0	0	770	940	90	10.444	1.70	1.427	235	28695
6808	2	2.647	306	2290.8	340.80	6.530	2.930	0	2	0	0	90	10.599	1.69	1.427	235	28699
6826	2	2.586	307	2294.6	335.00	6.528	2.941	0	4	1536	1830	90	10.348	1.71	1.425	236	28705
6812	2	2.850	308	2295.5	356.10	6.526	2.943	0	2	782	940	90	11.389	1.68	1.424	236	28710
6786	2	2.577	309	2299.9	135.40	6.522	2.956	0	0	854	1010	90	10.287	1.70	1.424	237	28711

TABLE 1 – RUN SUMMARY

Run Number	Diaphram	Freestream Pressure	Freestream Temperature	Freestream Velocity	Pitot Pressure	Mach Number	Total Enfalpy	Angle of Attack	Angle of Slew	Fuel Pressure Fpm	Initial Fuel Pressure Fpi	Shock Tube Fill Pressure	Stagnation Pressure	Shock Speed	Flight Pressure	Flight Temperature	Flight Altitude
Units	mm	kPa	K	ms^{-1}	kPa	-	$MJkg^{-1}$	degree	degree	kPa	kPa	kPa	MPa	kms^{-1}	kPa	K	m
6887	2	2.649	323	2337.5	149.40	6.489	3.057	2	0	646	980	90	10.499	1.76	1.424	245	28712
6824	2	2.777	312	2306.2	352.50	6.518	2.972	0	4	0	0	90	11.075	1.70	1.422	239	28722
6888	2	2.708	328	2350.2	152.40	6.478	3.090	2	0	625	760	90	10.639	1.76	1.420	248	28731
6828	2	2.688	313	2311.0	335.00	6.513	2.985	0	4	690	980	90	10.704	1.72	1.419	240	28735
6784	2	2.811	317	2322.1	143.30	6.503	3.014	0	0	914	1080	90	11.146	1.72	1.416	242	28750
6814	2	2.849	323	2336.9	348.50	6.491	3.056	0	2	604	760	90	11.250	1.73	1.411	246	28771
6813	2	2.874	324	2339.5	349.60	6.487	3.062	0	2	811	980	90	11.328	1.73	1.409	247	28783
6876	2	2.739	320	2329.5	141.60	6.496	3.035	-2	0	802	940	90	10.835	1.73	1.394	246	28849
6874	2	2.756	322	2335.9	142.50	6.491	3.051	-2	0	0	0	90	10.875	1.74	1.391	247	28865
6875	2	2.744	323	2337.0	142.40	6.491	3.054	-2	0	809	980	90	10.955	1.74	1.391	248	28865
6899	2	2.631	323	2336.5	142.20	6.491	3.053	-2	0	1224	1545	90	10.388	1.76	1.391	248	28865
6895	2	2.625	306	2289.2	137.00	6.532	2.927	-4	0	1350	1545	90	10.519	1.71	1.389	238	28873
6877	2	2.817	329	2353.3	147.10	6.475	3.099	-2	0	688	780	90	11.056	1.76	1.383	251	28905
6858	2	2.827	321	2333.8	133.20	6.493	3.046	-4	0	682	760	90	11.176	1.74	1.369	247	28970
6856	2	2.835	322	2335.3	132.30	6.492	3.051	-4	0	853	980	90	11.200	1.73	1.368	248	28977
6855	2	2.913	329	2354.3	132.10	6.475	3.102	-4	0	0	0	90	11.437	1.75	1.363	253	29000
6857	2	3.012	337	2375.3	139.10	6.456	3.160	-4	0	789	940	90	11.743	1.76	1.354	258	29044
6847	1	1.167	333	2365.2	58.25	6.464	3.132	4	0	297	300	34	4.564	1.74	0.745	250	33202
6837	1	1.077	315	2315.0	733.00	6.508	2.995	0	4	0	0	34	4.277	1.70	0.682	241	33809
6880	1	1.086	322	2334.3	56.23	6.491	3.047	-2	0	253	300	34	4.287	1.72	0.676	247	33871
6838	1	1.061	309	2298.9	141.50	6.522	2.953	0	4	276	300	34	4.234	1.68	0.676	237	33871
6839	1	1.059	309	2298.4	58.97	6.524	2.951	0	4	341	380	34	4.233	1.68	0.675	237	33881
6844	1	1.043	319	2324.2	58.20	6.500	3.021	4	0	0	0	34	4.130	1.72	0.674	241	33891
6849	1	1.102	328	2351.4	48.59	6.476	3.095	-4	0	0	0	34	4.330	1.74	0.673	252	33902
6879	1	1.050	309	2297.3	55.13	6.524	2.948	-2	0	347	380	34	4.195	1.68	0.660	238	34036
6890	1	1.026	313	2309.2	60.39	6.514	2.980	2	0	329	380	34	4.083	1.71	0.660	239	34036
6846	1	1.010	307	2293.1	48.68	6.528	2.938	4	0	329	380	34	4.042	1.69	0.659	233	34047
6891	1	1.009	311	2303.3	58.51	6.518	2.965	2	0	283	300	34	4.021	1.71	0.650	237	34142
6878	1	1.032	315	2315.1	54.02	6.508	2.996	-2	0	0	0	34	4.097	1.71	0.646	242	34184
6820	1	1.017	313	2309.8	128.70	6.513	2.982	0	2	0	0	34	4.045	1.71	0.646	240	34184
6823	1	1.001	304	2284.5	131.00	6.535	2.914	0	2	305	380	34	4.013	1.68	0.640	234	34249

TABLE 1 – RUN SUMMARY

Run Number	Diaphram	Freestream Pressure	Freestream Temperature	Freestream Velocity	Pitot Pressure	Mach Number	Total Enalpy	Angle of Attack	Angle of Slew	Fuel Pressure Fpm	Initial Fuel Pressure Fpi	Shock Tube Fill Pressure	Stagnation Pressure	Shock Speed	Flight Pressure	Flight Temperature	Flight Altitude
Units	mm	kPa	K	ms^{-1}	kPa	-	$MJkg^{-1}$	degree	degree	kPa	kPa	kPa	MPa	kms^{-1}	kPa	K	m
6889	1	0.977	312	2307.7	54.70	6.515	2.976	2	0	0	0	34	3.891	1.72	0.629	238	34370
6863	1	1.022	325	2343.0	49.12	6.484	3.071	-4	0	290	300	34	4.023	1.75	0.625	250	34414
6822	1	0.966	301	2275.9	128.00	6.542	2.892	0	2	272	300	34	3.883	1.68	0.620	232	34470
6789	1	0.960	309	2298.1	53.69	6.524	2.951	0	0	0	0	34	3.838	1.72	0.612	237	34560
6794	1	0.950	306	2288.9	52.62	6.531	2.926	0	0	266	300	34	3.802	1.71	0.607	235	34617
6792	1	0.931	307	2293.3	51.06	6.528	2.940	0	0	337	380	34	3.726	1.72	0.594	236	34768
6790	1	0.912	303	2280.9	48.52	6.538	2.905	0	0	0	0	34	3.663	1.71	0.584	233	34887
6788	1	0.906	298	2267.4	49.91	6.550	2.870	0	0	0	0	34	3.652	1.69	0.582	230	34911
6894	1	0.927	294	2253.8	48.76	6.561	2.835	-4	0	587	620	34	3.752	1.67	0.581	229	34923
6897	1	0.863	289	2242.0	46.17	6.572	2.803	-2	0	512	620	34	3.506	1.68	0.552	240	35282
6860	1	0.851	293	2252.8	45.65	6.562	2.832	-4	0	360	380	34	3.448	1.66	0.534	228	35515
6892	1	1.018	311	2305.4	48.02	6.516	4.041	-4	0	0	0	34	4.057	1.71	0.519	208	35716

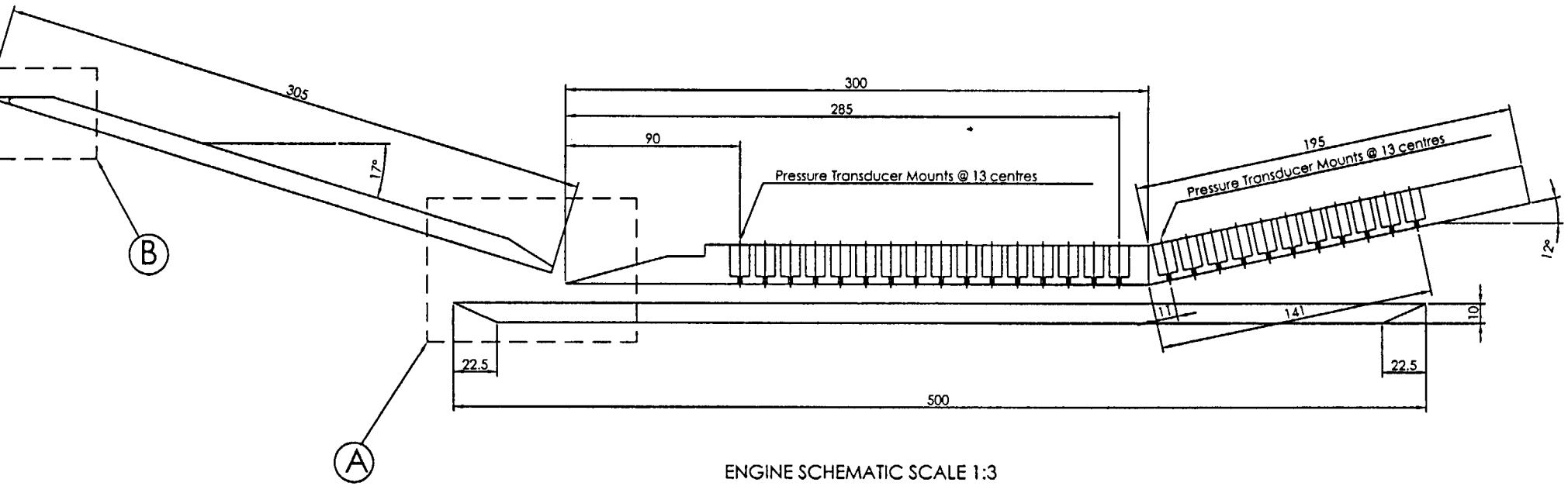

ENGINE SCHEMATIC SCALE 1:3

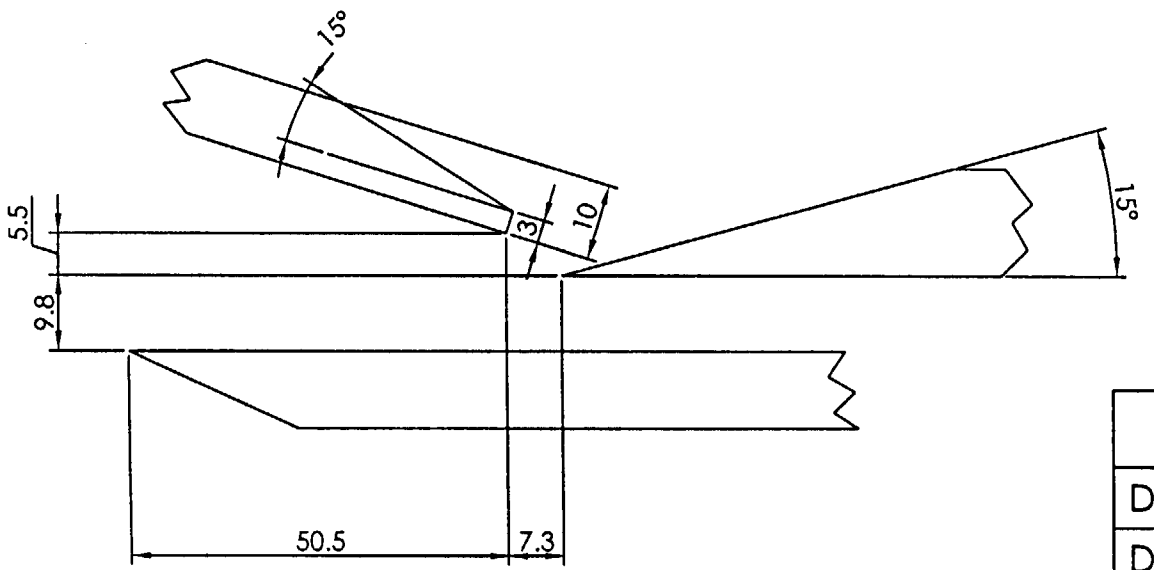

DETAIL A SCALE 1:2

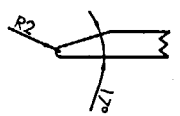

DETAIL B SCALE 1:3

UNIVERSITY OF QUEENSLAND		
DRAWN	M.FROST	HYSHOT
DATE	10 MAR 2000	
SCALE	AS SHOWN	PRIMARY DIMENSIONS
REV	0	ALL DIMENSIONS IN MM

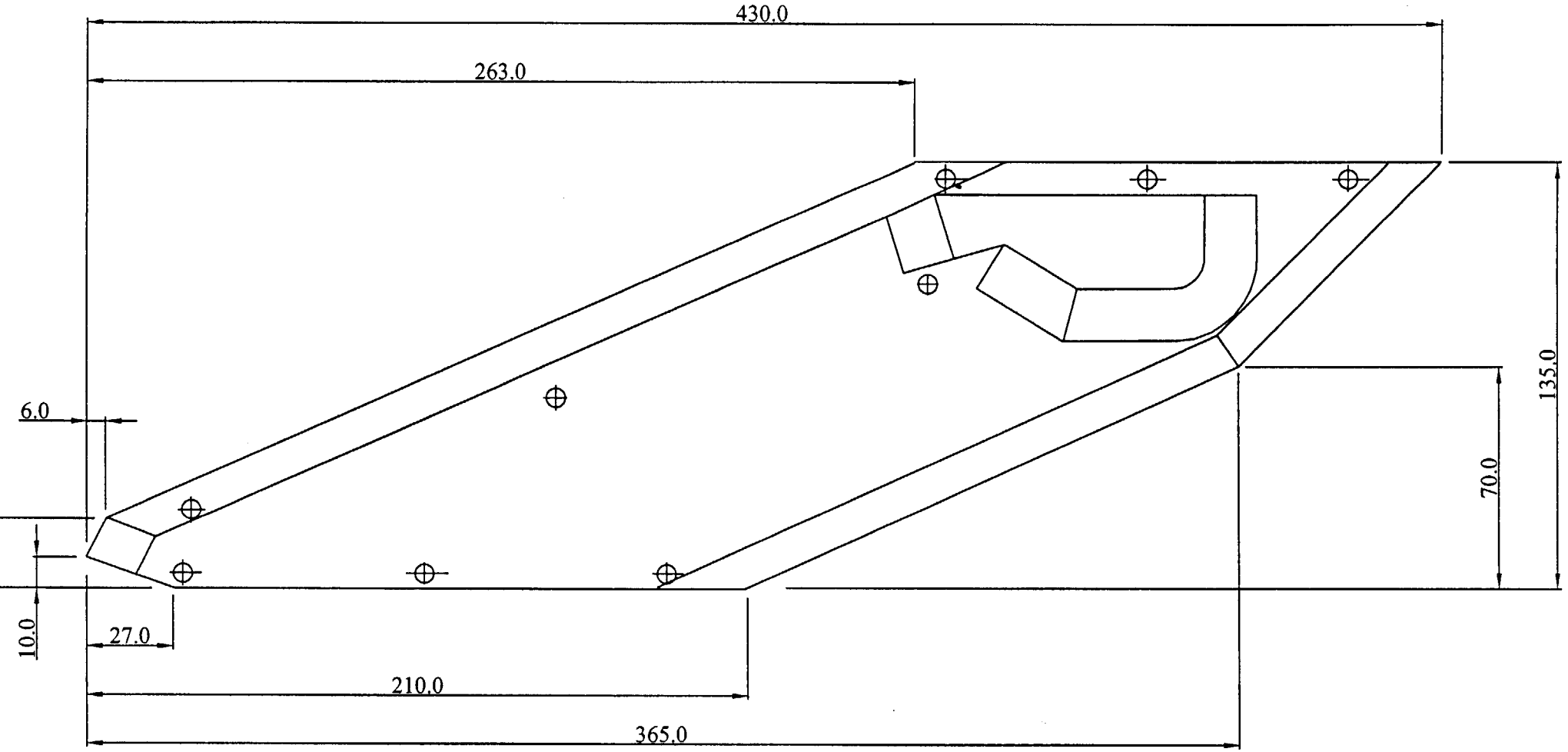

UNIVERSITY OF QUEENSLAND		
DRAWN	H.ALESI	HYSHOT
DATE	10 MAR 2000	
SCALE	NTS	INTAKE SIDEWALL
REV	0	EXTERNAL DIMENSIONS

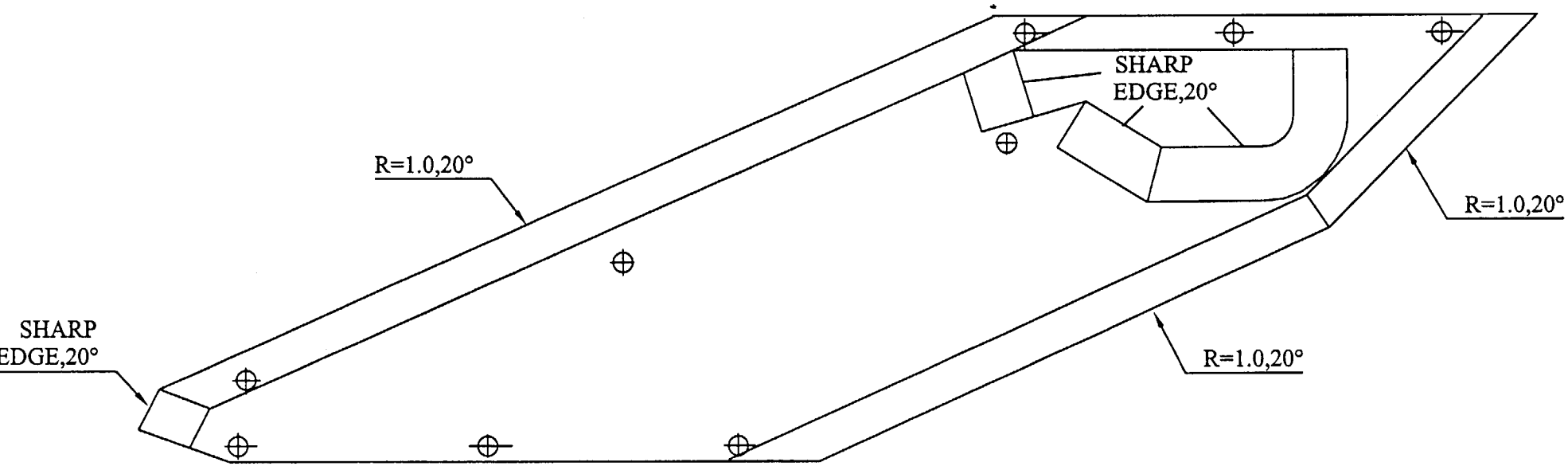

UNIVERSITY OF QUEENSLAND		
DRAWN	H.ALESI	HYSHOT
DATE	10 MAR 2000	
SCALE	NTS	INTAKE SIDEWALL
REV	0	EDGE DIMENSIONS

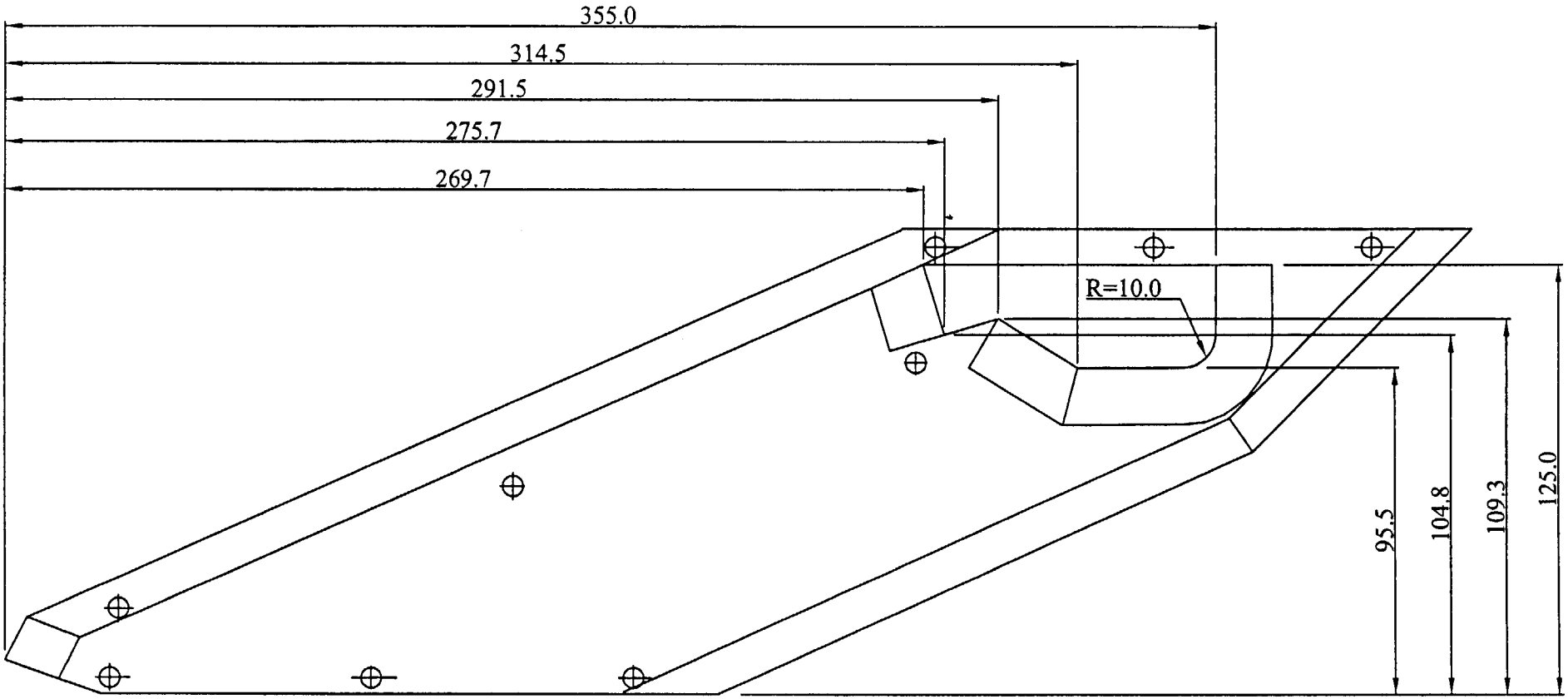

UNIVERSITY OF QUEENSLAND		
DRAWN	H.ALESI	HYSHOT
DATE	10 MAR 2000	
SCALE	NTS	INTAKE SIDEWALL
REV	0	CUTOUT DIMENSIONS

National Aeronautics and
Space Administration

Langley Research Center
100 NASA Road
Hampton, VA 23681-2199

y to Attn. of: 126

The University of Queensland
Brisbane, Queensland 4072
Australia

Subject: NASA Langley Research Center (LaRC) Research Grant NAG-1-2113-- Notice of Delinquent *Summary of Research* Report Submission (Principal Investigator: Dr. Allan Paull)

The purpose of this letter is to inform you that your institution is beyond the 90-day grace period allowed for the submission of the *Summary of Research* report required by the subject grant. The grant expired on 9/30/99.

Pursuant to the NASA Grant and Cooperative Agreement Handbook, Section 1260.21, a *Summary of Research* report is due within 90 days after the expiration of the grant, regardless of whether or not support is continued under another grant. There is no specified format for this report; however, it should include, as a minimum, a comprehensive summary of significant accomplishments made throughout the total period of the grant.

In as much as the *Summary of Research* report is the only deliverable required under the subject grant, it is imperative that the LaRC Grant Office, Mail Stop 126, receive this report. Copies of the report should also be submitted to MS 168, Dr. Aaron H. Auslender, LaRC Technical Officer, and to the NASA Center for AeroSpace Information (CASI). The CASI copy should be easily reproducible (i.e., one-sided, no-staples, and no-binder) and should be submitted to the following address:

NASA Center for AeroSpace Information (CASI)
7121 Standard Drive
Hanover, MD 21076-1320

If the *Summary of Research* report has not been submitted to the undersigned by **April 18, 2000**, the Center will withhold all future grants, grant supplements, and/or payments to your institution. You should contact the LaRC Grant Administrator, Ms. Carol Reddic, within 1 week of receipt of this letter to make arrangements for submitting this delinquent report . Ms. Reddic can be reached by phone at (757) 864-6042. If you have other questions regarding this requirement, contact me at (757) 864-2477 or e-mail me at r.t.lacks@larc.nasa.gov.

R. Todd Lacks
LaRC Grant Officer

Please, find enclosed the appropiate report.